iScience

CellPress
OPEN ACCESS

Article

Propionate induces intestinal oxidative stress via Sod2 propionylation in zebrafish

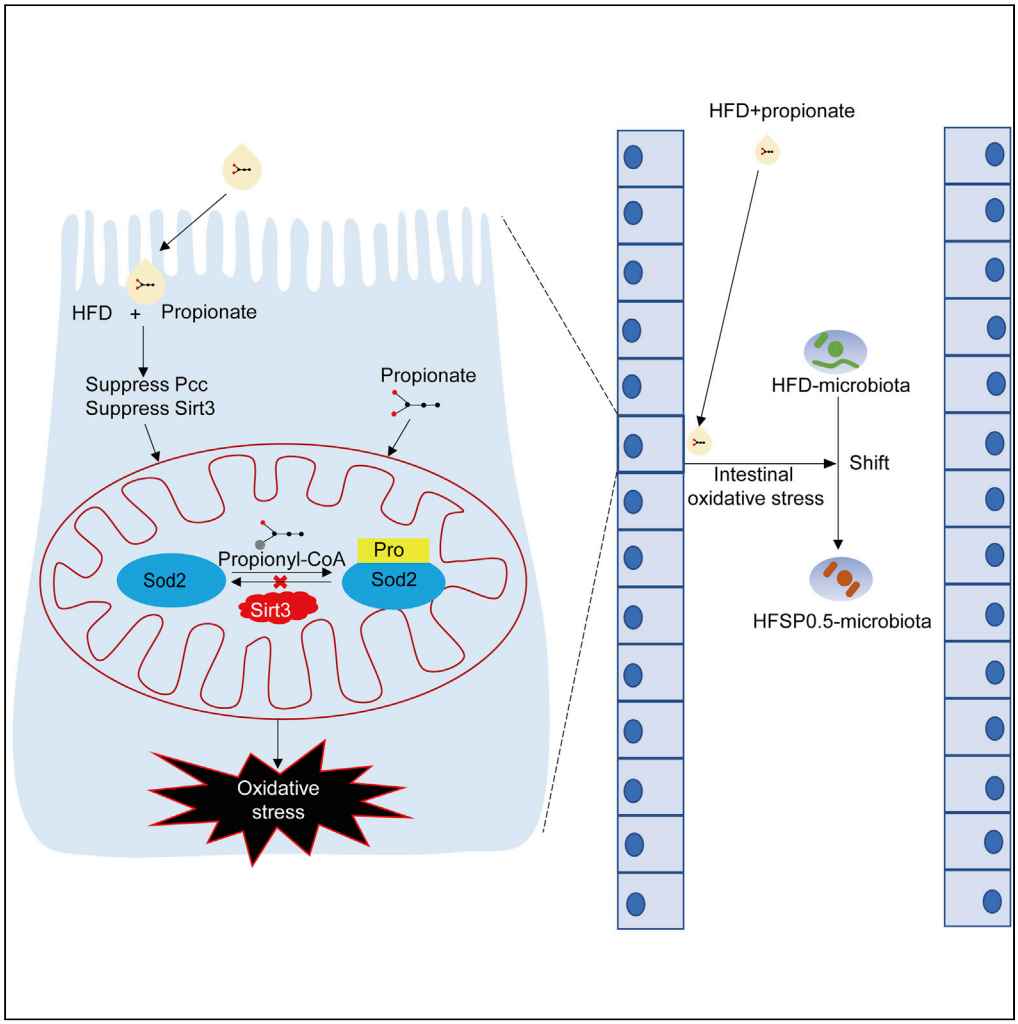

Qianwen Ding, Zhen Zhang, Yu Li, ..., Jihong Liu Clarke, Chao Ran, Zhigang Zhou

ranchao@caas.cn (C.R.)
zhouzhigang03@caas.cn (Z.Z.)

Highlights

Propionate supplementation in high-fat diet induces intestinal damage

Propionate induces oxidative stress via Sod2 propionylation at 132 lysine site

Increased Sod2 propionylation is associated with reduced expression of Sirt3

Intestinal oxidative stress alters gut microbiota composition

Ding et al., iScience 24, 102515
June 25, 2021
https://doi.org/10.1016/j.isci.2021.102515

iScience

CellPress
OPEN ACCESS

Article

Propionate induces intestinal oxidative stress via Sod2 propionylation in zebrafish

Qianwen Ding,[1,2] Zhen Zhang,[3] Yu Li,[1] Hongliang Liu,[1] Qiang Hao,[1] Yalin Yang,[3] Einar Ringø,[2] Rolf Erik Olsen,[2] Jihong Liu Clarke,[4] Chao Ran,[3,*] and Zhigang Zhou[1,5,*]

SUMMARY

Propionate and propionyl-CoA accumulation have been associated with the development of mitochondrial dysfunction. In this study, we show that propionate induces intestinal damage in zebrafish when fed a high-fat diet (HFD). The intestinal damage was associated with oxidative stress owing to compromised superoxide dismutase 2 (Sod2) activity. Global lysine propionylation analysis of the intestinal samples showed that Sod2 was propionylated at lysine 132 (K132), and further biochemical assays demonstrated that K132 propionylation suppressed Sod2 activity. In addition, sirtuin 3 (Sirt3) played an important role in regulating Sod2 activity via modulating de-propionylation. Finally, we revealed that intestinal oxidative stress resulting from Sod2 propionylation contributed to compositional change of gut microbiota. Collectively, our results in this study show that there is a link between Sod2 propionylation and oxidative stress in zebrafish intestines and highlight the potential mechanism of intestinal problems associated with high propionate levels.

INTRODUCTION

Propionate is a ubiquitous short-chain fatty acid (SCFA). It is a common food preservative widely used in the food industry and agriculture including many fish feeds (Rose, 2013). The maximum inclusion level is up to 0.5% (Rose, 2013). Meanwhile, propionate is one of the major fermentation products of the enteric microbiome (Koh et al., 2016). Thus human and animals are exposed to propionate derived from both endogenous and nutritional sources.

As an SCFA, propionate will cross the mitochondrial inner membrane and serve as precursor for generation of propionyl-CoA, which could enter the tricarboxylic acid (TCA) cycle for energy metabolism. Propionyl-CoA can also act as donor for lysine propionylation (Schonfeld and Wojtczak, 2016; Flavin and Ochoa, 1957; Chen et al., 2007; Cheng et al., 2009). Lysine propionylation is a common posttranslational modification (PTM) occurring in histones of eukaryotic cells (Chen et al., 2007; Cheng et al., 2009; Liu et al., 2009; Zhang et al., 2009). Similar to acetylation and butyrylation, histone propionylation is a marker of active chromatin (Kebede et al., 2017). Furthermore, the presence of lysine propionylation in non-histone proteins such as p53, p300, and cAMP response element-binding protein has been reported in 293T cells (Cheng et al., 2009). Although the role of lysine propionylation in non-histone proteins of eukaryotic cells is rarely reported, existing evidences in bacteria suggest a role similar to lysine acetylation in modulating protein function (Starai et al., 2002; Garrity et al., 2007).

Mitochondria are both the source and target of reactive oxygen species (ROS). Impaired mitochondrial respiration will increase ROS production (Bhatti et al., 2017). Excessive ROS accumulation causes oxidative stress, which in turn leads to mitochondrial dysfunction (Bhatti et al., 2017; Wei et al., 1998; Duchen, 2004; Pieczenik and Neustadt, 2007). Propionate may inhibit mitochondrial respiration due to significant propionyl-CoA accumulation (Matsuishi et al., 1991; Schwab et al., 2006). Propionyl-CoA accumulation inhibits the activity of mitochondrial respiration complexes, which implicates the involvement of protein propionylation (Lagerwaard et al., 2020). However, the potential links between protein propionylation and oxidative stress have never been studied.

The intestinal epithelium is particularly prone to oxidative damage induced by luminal oxidants because it locates at the interface between the intestinal tissue and luminal environment (Circu and Aw, 2012). In the

[1]China-Norway Joint Lab on Fish Gastrointestinal Microbiota, Institute of Feed Research, Chinese Academy of Agricultural Sciences, Beijing 100081, China

[2]Norway-China Joint Lab on Fish Gastrointestinal Microbiota, Institute of Biology, Norwegian University of Science and Technology, Trondheim 7491, Norway

[3]Key Laboratory for Feed Biotechnology of the Ministry of Agriculture and Rural Affairs, Institute of Feed Research, Chinese Academy of Agricultural Sciences, Beijing 100081, China

[4]NIBIO, Norwegian Institute of Bioeconomy Research, Ås 1431, Norway

[5]Lead contact

*Correspondence: ranchao@caas.cn (C.R.), zhouzhigang03@caas.cn (Z.Z.)

https://doi.org/10.1016/j.isci.2021.102515

current study, we observed that propionate induced oxidative damage to zebrafish intestine when fed a high-fat diet (HFD). We established a plausible mechanism underlying propionate-induced intestinal oxidative damage that involved propionylation of superoxide dismutase 2 (Sod2) at the lysine 132 site (K132), which suppressed its activity and resulted in oxidative damage in the intestine. Furthermore, we found that increased propionylation of Sod2 was linked to reduced intestinal expression of sirtuin 3 (Sirt3) in zebrafish fed high fat plus propionate diet.

RESULTS

Propionate supplementation in high-fat diet induces intestine damage in zebrafish

We established a propionate-feeding model by feeding one-month-old zebrafish a series of low- (6% oil) and high (16% oil)-fat diets with 0, 0.25, 0.5, and 1.0% propionate. Both LFD (low fat no propionate) and HFD (high fat no propionate) were tested, as HFD has been a very common basal dietary condition for both human and animals (Du et al., 2014; Zhai et al., 2014; Shapawi et al., 2014). The diets were designated LFD, LFSP0.25, 0.5, and 1.0 for low-fat propionate-supplemented diets and similarly HFD, HFSP0.25, 0.5, and 1.0 for the corresponding HFD. The he zebrafish were fed these diets for 2 weeks (Figure S1; Tables S1 and S2). After 2-week feeding trial, propionate supplementation in LFD showed no effect on zebrafish weight gain and feed efficiency (Figures S1A and S1B), and mortality of LFSP1.0-fed zebrafish was significantly decreased when challenged by *Aeromonas veronii* (*A. veronii* Hm091) (Figure S1C). In the context of HFD, propionate supplementation decreased weight gain and feed efficiency at both 0.5% and 1.0% when compared with zebrafish fed the HFD (Figure S1D). Feed efficiency also tended to be reduced, but was only significant for the HFSP0.5 group (Figure S1E). Mortality following challenge with *A. veronii* Hm091 tended to increase when propionate was added to the diet but was only statistically significant for the HFSP0.5-fed zebrafish (Figure S1F).

At the end of feeding, serum endotoxin level was increased by 70.8% (Figure 1A), and the relative mRNA expression of *claudin-15* and *occludin* was significantly reduced in HFSP0.5-fed zebrafish as compared with the HFD group (Figures 1B and 1C). This suggests that 0.5% propionate-supplemented HFD might impair intestinal barrier function. Histopathologic examination of intestinal sections showed considerable morphological damage (i.e., breaches in the intestinal epithelium and injury to or loss of intestinal villi) in the HFSP0.5 group compared with those fed HFD (Figures 1D and 1E). These evidences together indicate that dietary propionate induces intestinal damage in the context of HFD. The activity of caspase-9, caspase-6, and caspase-3 were 16.7% (Figure 1F), 29.6% (Figure 1G), and 45.7% (Figure 1H) higher, respectively, in intestines of HFSP0.5-fed zebrafish compared with those fed the HFD, suggesting that a mitochondrial pathway of apoptosis was activated in the HFSP0.5 group. Intestinal caspase-8 and caspase-12 activities were similar in HFSP0.5 and HFD-fed zebrafish (Figures S2A and S2B). In this respect, it is worth noting that 0.5% propionate-supplemented LFD had little or no effect on damage markers such as serum endotoxin content, junctional proteins expression, histological score (Figures 1A–1E), or intestinal caspase-9 and caspase-3 activities (Figure S2C). The results clearly indicate that 0.5% propionate might only cause intestinal damages when accompanied by HFD. From this point, comparisons were only made for the selected groups, mainly LFD, HFD, and HFSP0.5. Thus the following studies aimed to study the mechanisms behind the negative effects of propionate on the intestine of zebrafish fed HFD.

Propionate induces intestinal oxidative stress in zebrafish fed high-fat diet

Analysis of intestinal oxidative stress markers showed that mitochondrial ROS (Figure 2A), malonaldehyde (MDA) (Figure 2B), and protein carbonyl (PC) content (Figure 2C) increased by 49.1%, 17.7%, and 87.5%, respectively, in zebrafish fed HFSP0.5 when compared with those maintained on HFD, suggesting the induction of intestinal oxidative stress of dietary propionate in the context of HFD. In contrast, zebrafish fed LFSP0.5 showed similar intestinal ROS to the counterparts fed LFD (Figure S3). The total antioxidant capability (T-AOC) (Figure 2D) and Sod2 activity (Figure 2E) in intestines of HFSP0.5-fed zebrafish were reduced by 22.4% and 43.5%, respectively, as compared with that in HFD-fed zebrafish. However, there were no dietary effects on the activity of other intestinal antioxidant enzymes, such as glutathione peroxidase (Gpx) (Figure 2F) and catalase (Cat) (Figure 2G). Furthermore H&E-stained intestinal sections of HFSP0.5-fed zebrafish administrated 4-hydroxy-TEMPO, an SOD mimic, showed less damage than saline-administered control (Figures 2H and 2I). Taken together, these results indicate that the intestine-damaging effect of HFSP0.5 was due to impaired T-AOC and oxidative stress, which may be at least partially attributable to the inhibition of Sod2 activity.

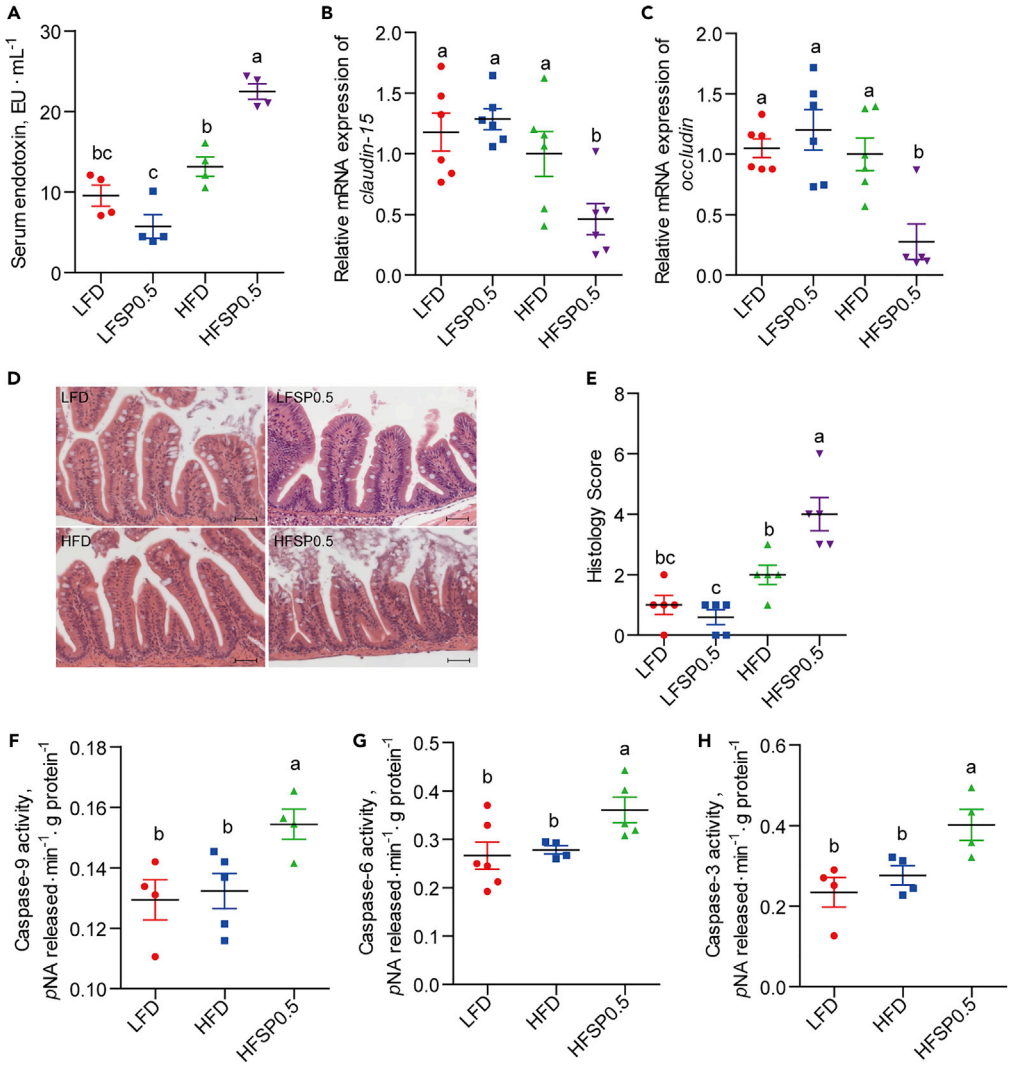

Figure 1. Propionate induces intestinal damage in the context of high-fat diet

(A) Serum endotoxin in LFD-, LFSP0.5-, HFD-, and HFSP0.5-fed zebrafish at the end of the 2-week feeding trial (n = 4).

(B and C) The relative mRNA expression of (B) *claudin-15* and (C) *occludin* in the intestine of LFD-, LFSP0.5-, HFD-, and HFSP0.5-fed zebrafish at the end of 2-week feeding trial (n = 5–6).

(D) Representative histopathologic image of H&E-stained intestinal sections. The scale bar, 50 μm.

(E) Histological score measuring the severity of the intestinal damage of zebrafish (n = 5).

(F–H) (F) Caspase-9, (G) caspase-6, and (H) caspase-3 activities in the intestine of 1-month-old zebrafish fed the LFD, HFD, or HFSP0.5 for 2 weeks (n = 4–6).

Values are means ± SEM. Means without a common letter are significantly different ($p < 0.05$). Duncan's test. LFD, low-fat diet; LFSP0.5, 0.5% propionate-supplemented LFD; HFD, high-fat diet; HFSP0.5, 0.5% propionate-supplemented HFD. See also Figures S1and S2.

To further validate the effect of propionate on intestinal epithelium, we established an oleic acid-palmitic acid-propionate (OPP) model using the ZF4 cell line where the cells were treated with a mixture of 150 μM oleic acid and 50 μM palmitic acid (OPA) or a mixture of 150 μM oleic acid, 50 μM palmitic acid, and propionate (1, 5, 10 or 50 mM) (OPP1/5/10/50). In this model, OPA treatment acted as the high fat control. In the context of OPA, the effects of propionate on ZF4 cell viability, cell apoptosis, ROS, and Sod2 activity were evaluated. We observed a concentration-dependent decrease of cell survival rate (7.2%–24. 9%) (Figure 3A) and increase of cell apoptotic rate (15.7%–31.4%) (Figure 3B) after OPP treatment for 24 h. The relative cellular ROS levels examined by a fluorescence microplate reader increased by 1.1-, 1.3-, 1.5- and 2.4-fold in the OPP1, OPP5, OPP10, and OPP50 treatments, respectively, as compared with

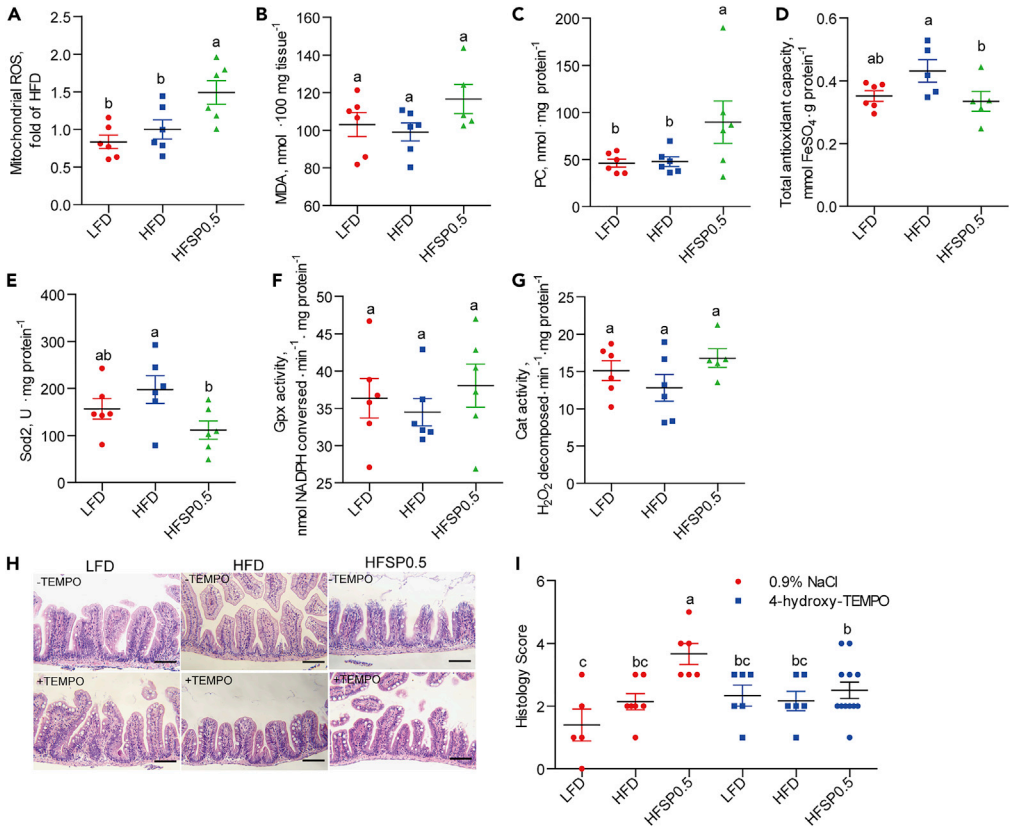

Figure 2. Propionate induces intestinal oxidative stress in the context of high-fat diet

(A–C) Intestinal biomarkers for oxidative stress in 1-month-old zebrafish fed the LFD, HFD, or HFSP0.5 for 2 weeks, including (A) mitochondrial ROS, (B) MDA, and (C) PC.

(D) Intestinal total antioxidant capability in 1-month-old zebrafish fed LFD, HFD, or HFSP0.5 for 2 weeks.

(E–G) Intestinal antioxidant enzymes in 1-month-old zebrafish fed the LFD, HFD, or HFSP0.5 for 2 weeks, including (E) Sod2, (F) Gpx, and (G) Cat.

(H) Representative histopathologic images of H&E-stained intestinal sections in zebrafish intraperitoneally injected with 4-hydroxy-TEMPO, a membrane-permeable radical scavenger. The scale bar, 50 μm.

(I) Histological score measuring the severity of the intestinal damage of zebrafish intraperitoneally injected with 4-hydroxy-TEMPO.

Values are means ± SEM (n = 5–12). Means without a common letter are significantly different ($p < 0.05$). Duncan's test. See also Figure S3.

OPA-treated ZF4 cells (Figure 3C). The mean fluorescence intensity of the ROS signal acquired by flow cytometry was 60.3%, 89.0%, 125.5%, and 214.0% higher in OPP1-, OPP5-, OPP10-, and OPP50-treated ZF4 cells, respectively, compared with the OPA controls (Figure 3D and 3E). The Sod2 activity in OPP1-, OPP5-, OPP10-, and OPP50-treated ZF4 cells was inhibited by 17.5%, 42.2%, 45.3%, and 57.7% as compared with OPA controls (Figure 3F).

Propionate induces Sod2 propionylation at 132 lysine site

Propionate induced hyper-propionylation of intestinal mitochondrial proteins in zebrafish fed the HFSP0.5 (Figure S4; Table S3). HPLC-MS/MS-based proteomics analysis identified a Sod2 peptide, DFGSFQK$_{+57.0901}$MN, with a mass shift of +57.0901 Da at the K132 in the intestine of HFSP0.5-fed zebrafish as compared with that in HFD-fed zebrafish (Figure 4A; Table S4). Despite the fact that Sod2 activity was reduced in the HFSP0.5 group when compared with HFD group, the total protein level of intestinal Sod2 was similar in both groups (Figure 4B). Immunoblotting using an anti-propionyl-K132 Sod2 antibody demonstrated increased propionylation of Sod2 K132 in the intestine from HFSP0.5-fed zebrafish as compared with HFD-fed zebrafish (Figure 4B). Consistently, the propionylation of Sod2 K132 was enhanced by exposure to OPP in ZF4 cells (Figure 4C). His-Sod2 overexpressed and immunoprecipitated from

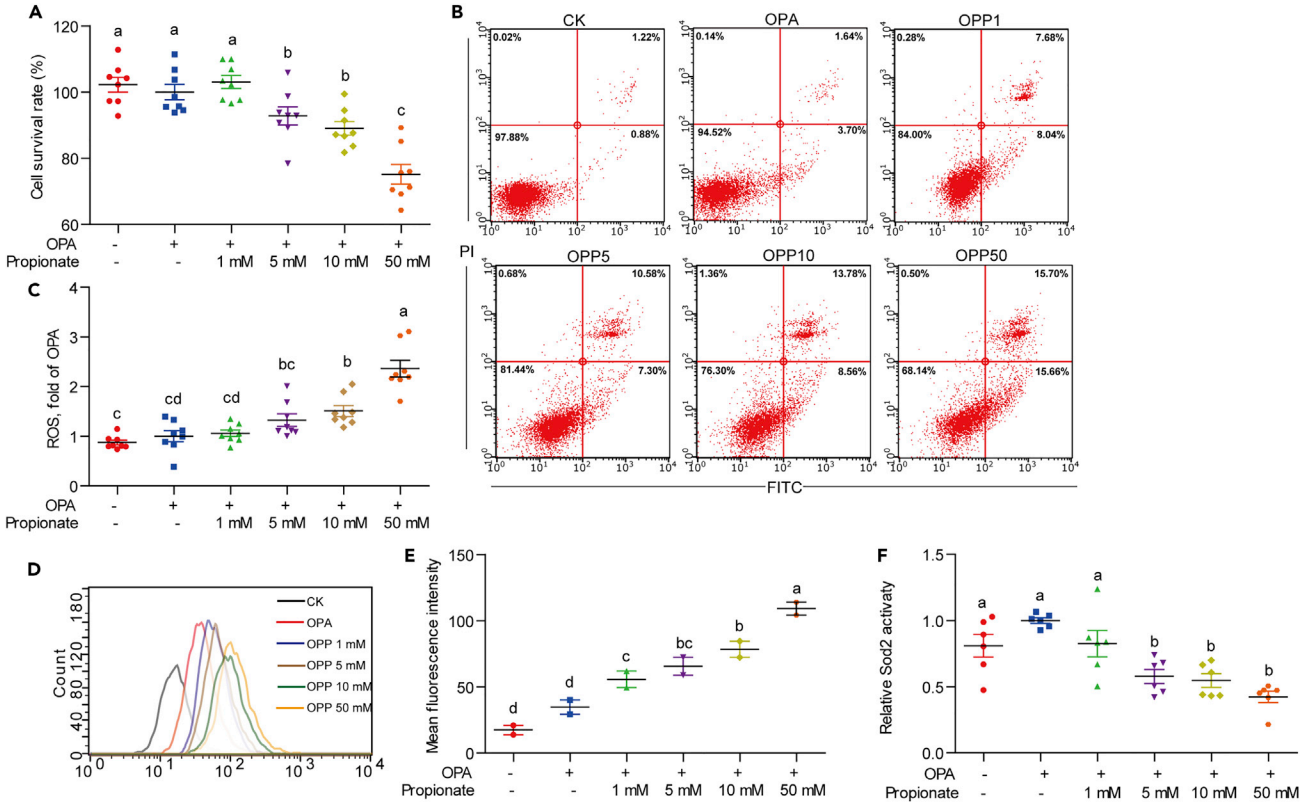

Figure 3. ZF4 cell model validating the cytotoxicity of propionate and its role on Sod2 activity

(A) Cell survival rate in ZF4 cells treated with OPA or a mixture of OPA with increasing concentrations of propionate for 24 h (n = 8).

(B) Representative plot of cell apoptotic rate in ZF4 cells treated with OPA or a mixture of OPA with increasing concentrations of propionate (OPP1, OPP5, OPP10, and OPP50) for 24 h.

(C) Relative amount of cellular ROS acquired by a fluorescence microplate reader between ZF4 cells treated with OPA or a mixture of OPA with increasing concentrations of propionate for 24 h (n = 8).

(D) DCFH-DA histogram acquired by flow cytometry between ZF4 cells treated with OPA or mixtures of OPA with increasing concentrations of propionate for 24 h.

(E) Mean fluorescence intensity of DCFH-DA in ZF4 cells treated with OPA or a mixture of OPA with increasing concentrations of propionate for 24 h (n = 2).

(F) Sod2 activity in ZF4 cells treated with OPA or a mixture of OPA with increasing concentrations of propionate for 24 h (n = 6).

Values are means ± SEM. Means without a common letter are significantly different ($p < 0.05$). Duncan's test.

HEK293 cells were subject to HPLC-MS/MS analysis. Results showed that his-Sod2 overexpressed in OPA-treated HEK293 cells were acetylated in K70, K77, and K132, whereas that overexpressed in OPP50-treated HEK293 cells showed no significant alteration in acetylation level but acquired extra propionylation at K132 (Figure 4D and Table 1). Moreover, his-Sod2 overexpressed in HEK293 cells could be readily propionylated at K132 by adding propionyl-CoA in a dose-dependent manner (Figure 4E), confirming that Sod2 K132 could be propionylated. Compared with LFD-fed zebrafish, the mRNA level of the *pcca* subunit was reduced in the intestines of zebrafish fed HFD and HFSP0.5 (Figure 4F), whereas the expression of the *pccb* subunit was similar in the LFD and HFD groups but reduced in HFSP0.5 group (Figure 4F).

Sod2 propionylation at 132 lysine site accounts for cellular ROS increase

To determine whether propionylation at K132 compromises the activity of Sod2, we generated plasmids expressing mutated zebrafish flag-Sod2 in which K132 was substituted by arginine (R, conserves the positive charge) or glutamine (Q, mimics lysine propionylation) (K132R/Q). The plasmids were then transfected into ZF4 cells with endogenous Sod2 knock-down. *Si*RNA (mixture of *sod2*-57 and *sod2*-412) targeting *sod2* was used to reduce its expression in ZF4 cells, and scrambled *si*RNA was used as a negative control (Figure S5 and Table S5). This resulted in reduced cell viability and elevated ROS (Figure S6). The results showed that overexpression of WT Sod2 and Sod2 K132R/Q compensated the protein content of Sod2 (Figure 5A). Compared with the ZF4 cells transfected with WT Sod2, cells transfected with the Sod2

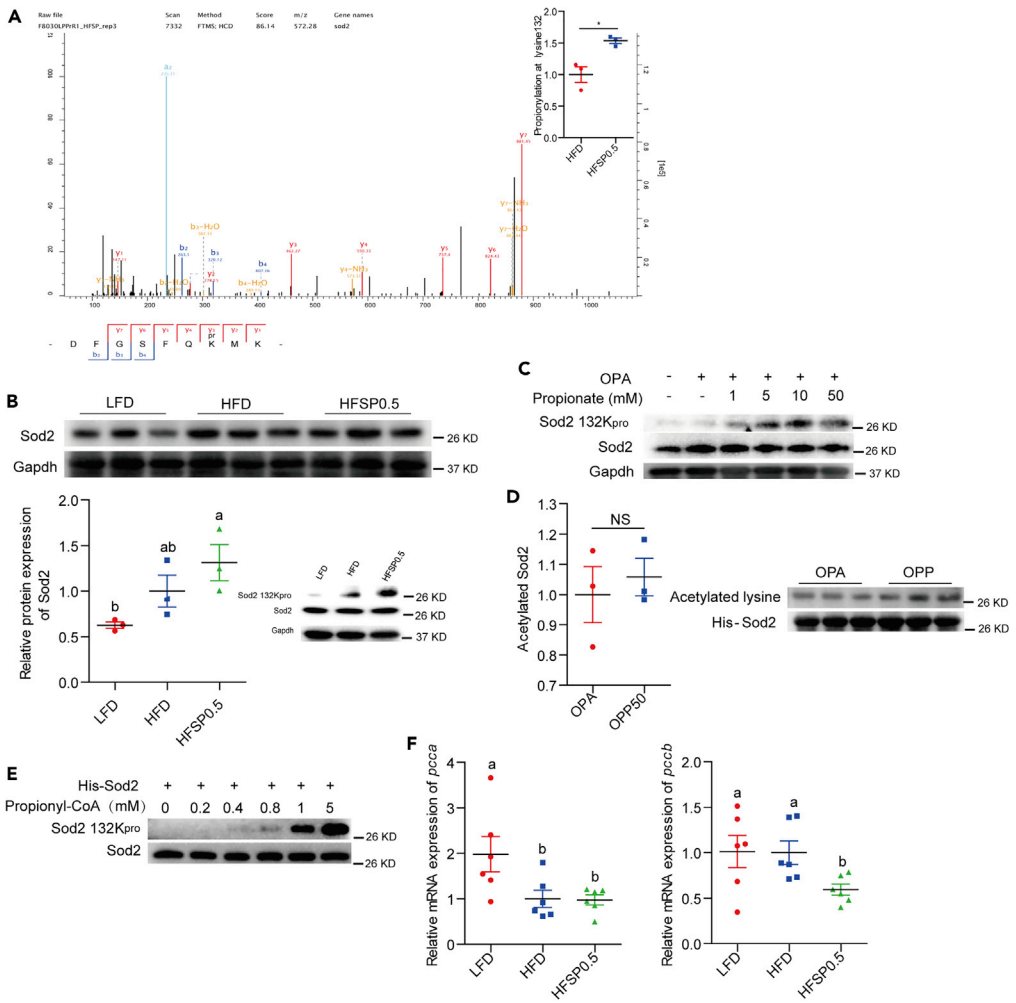

Figure 4. Propionate contributes to Sod2 propionylation at 132 lysine site in zebrafish fed high-fat diet

(A) HPLC-MS/MS spectra of an Sod2 peptide bearing propionylation (DFGSFQK$_{+57.0901}$MN).

(B) A representative western blotting showing patterns of Sod2 expression and Sod2 propionylation at the K132 and quantification of intestinal Sod2 protein level in zebrafish fed LFD, HFD, or HFSP0.5 for 2 weeks (n = 3).

(C) A representative western blotting showing patterns of Sod2 expression and Sod2 propionylation at the K132 in ZF4 cells treated with OPA or OPP.

(D) Western blotting showing the pattern of his-Sod2 acetylation purified from OPA- or OPP-treated HEK293 cells (n = 3).

(E) A representative western blotting showing the pattern of his-Sod2 propionylation at K132 incubated with the indicated concentrations of propionyl-CoA.

(F) The mRNA expression of genes encoding subunits of intestinal Pcc, an enzyme catalyzing the carboxylation of propionyl-CoA, in zebrafish fed HFD or HFSP0.5 for 2 weeks (n = 6).

Values are means ± SEM. A and D were analyzed by Student's t test, *, $p < 0.05$, NS, not significant. B and F were analyzed by Duncan's test and means without a common letter are significantly different ($p < 0.05$).

See also Figure S4.

K132R mutant had similar Sod2 activity, ROS level, and cell viability (Figures 5B–5D), whereas cells transfected with Sod2 K132Q mutant had a 31.9% reduction in Sod2 activity (Figure 5B), 30.0% elevation in ROS level (Figure 5C), and 30.0% inhibition in cell viability (Figure 5D). These results indicated that K132 is a key site for Sod2 activity, and propionylation at K132 compromises the Sod2 activity, leading to enhanced ROS. Moreover, ZF4 cells overexpressed Sod2 K132R (without Sod2 knock-down), maintained the Sod2 activity (Figure 5E), and prevented increase in cellular ROS (Figure 5F) after OPP50 treatment when compared with cells overexpressed with WT Sod2. This supports the finding that Sod2 K132 propionylation reduces Sod2 activity, which leads to enhanced ROS under high fat plus propionate conditions.

Table 1. Modified lysine site in purified his-Sod2

Group	Modification type	Peptide modified	Site
OPA	Acetylation	YQEALAK$_{Ac}$GDVTTQVSLQPALK	K77
		HHATYVNNLNVTEEK$_{Ac}$YQEALAK	K70
		DFGSFQK$_{Ac}$MK	K132
OPP50	Acetylation	YQEALAK$_{Ac}$GDVTTQVSLQPALK	K77
		HHATYVNNLNVTEEK$_{Ac}$YQEALAK	K70
		DFGSFQK$_{Ac}$MK	K132
	Propionylation	DFGSFQK$_{Pro}$MK	K132

Ac, acetylation site; Pro, propionylation site. K, lysine; OPA, mixture of 150 μM oleic acid and 50 μM palmitic acid; OPP50, mixture of 150 μM oleic acid, 50 μM palmitic acid, and 50 mM propionate.

Collectively, these results indicate that propionylation of Sod2 at K132 inhibits Sod2 activity and accounts for cellular ROS accumulation.

Inhibition of Sirt3 promotes Sod2 propionylation

Recent studies have shown that the sirtuin family of deacetylases have de-propionylation activity (Bheda et al., 2011). We evaluated the expression of genes encoding sirtuins in zebrafish intestine among zebrafish fed HFD and HFSP0.5. The relative expression of mRNA encoding intestinal *sirt3* was reduced by 48.1% in zebrafish fed HFSP0.5 as compared with those fed HFD (Figure S7A). This observation was confirmed by immunoblotting with an anti-Sirt3 antibody, which showed a clear reduction in Sirt3 protein level in the intestine of HFSP0.5-fed zebrafish as compared with HFD-fed counterparts (Figures 6A and S7B). Moreover, the relative mRNA expression of *sirt3* in ZF4 cells treated with OPP50 was 42.8% lower than that in OPA-treated cells (Figure 6B). To identify whether Sirt3 reduction was associated with propionylation of intestinal Sod2 at the K132 site, we knocked down *sirt3* with *si*RNA (mixture of *sirt3*-391, *sirt3*-755 and *sirt3*-885) in ZF4 cells (Figure S8 and Table S5). Immunoblotting with anti-propionyl-K132 Sod2 antibody showed that knockdown of *Sirt3* increased propionylation of Sod2 at K132 (Figure 6C). In agreement with increased propionylation of Sod2 at K132 in *sirt3*-knockdowned ZF4 cells, cell viability and Sod2 activity were decreased by 28.1% and 27.2%, respectively (Figures 6D and 6E). Together, these results indicate that Sirt3 plays an important role in regulating Sod2 activity via modulating propionylation at K132.

Intestinal oxidative stress induced by Sod2 propionylation disturbs gut microbiota composition

The composition of gut microbiota was assessed via 16S *r*RNA gene sequencing. In HFD-fed zebrafish, the relative abundance of Proteobacteria, Fusobacteria, and Firmicutes were 73.8%, 4.7%, and 15.9%, respectively (Figure 7A and Table 2), whereas it changed to 89.7%, 1.3%, and 6.8%, respectively, in HFSP0.5-fed zebrafish (Figure 7A and Table 2). The relative abundance of *Plesiomonas* in HFD-fed zebrafish was 18.3% (Figure 7B and Table 3), which increased to 51.4% in HFSP0.5-fed zebrafish (Figure 7B, Table 3). Although the relative abundance of *Cetobacterium* was 4.6% in HFD-fed zebrafish, it was reduced to only 1.2% in HFSP0.5-fed zebrafish (Figure 7B, Table 3). The total bacterial counts were comparable in gut contents from zebrafish fed HFD and HFSP0.5 (Figure 7C). These results indicate that Proteobacteria and *Plesiomonas* are enriched in the intestine of HFSP0.5-fed zebrafish, whereas the abundance of Firmicutes and *Cetobacterium* are reduced.

To examine the contribution of oxidative stress to the altered composition of gut microbiota, we cultured gut microbiota isolated from HFD-fed zebrafish in GAM containing 2 mmol/L H_2O_2 for 48 h and evaluated the effect of H_2O_2 on gut microbiota alteration. The results showed that the number of Fusobacteria, Firmicutes, and *Cetobacterium* were dramatically reduced (Figures 7D and 7E), whereas the number of *Plesiomonas* increased (Figures 7D and 7E). Adding 0.5 mg/mL of the antioxidant lipoic acid (LA) to the medium partially recovered the number of Fusobacteria, Firmicutes, and *Cetobacterium* and restricted the growth of *Plesiomonas* (Figures 7D and 7E). These results indicate that oxidative stress contributes to the compositional change of gut microbiota in an *ex vivo* culture system.

To study the transfer value of oxidative stress to gut microbiota *in vivo*, we performed *q*PCR analysis to determine the number of Proteobacteria and *Plesiomonas* in gut content collected from zebrafish fed

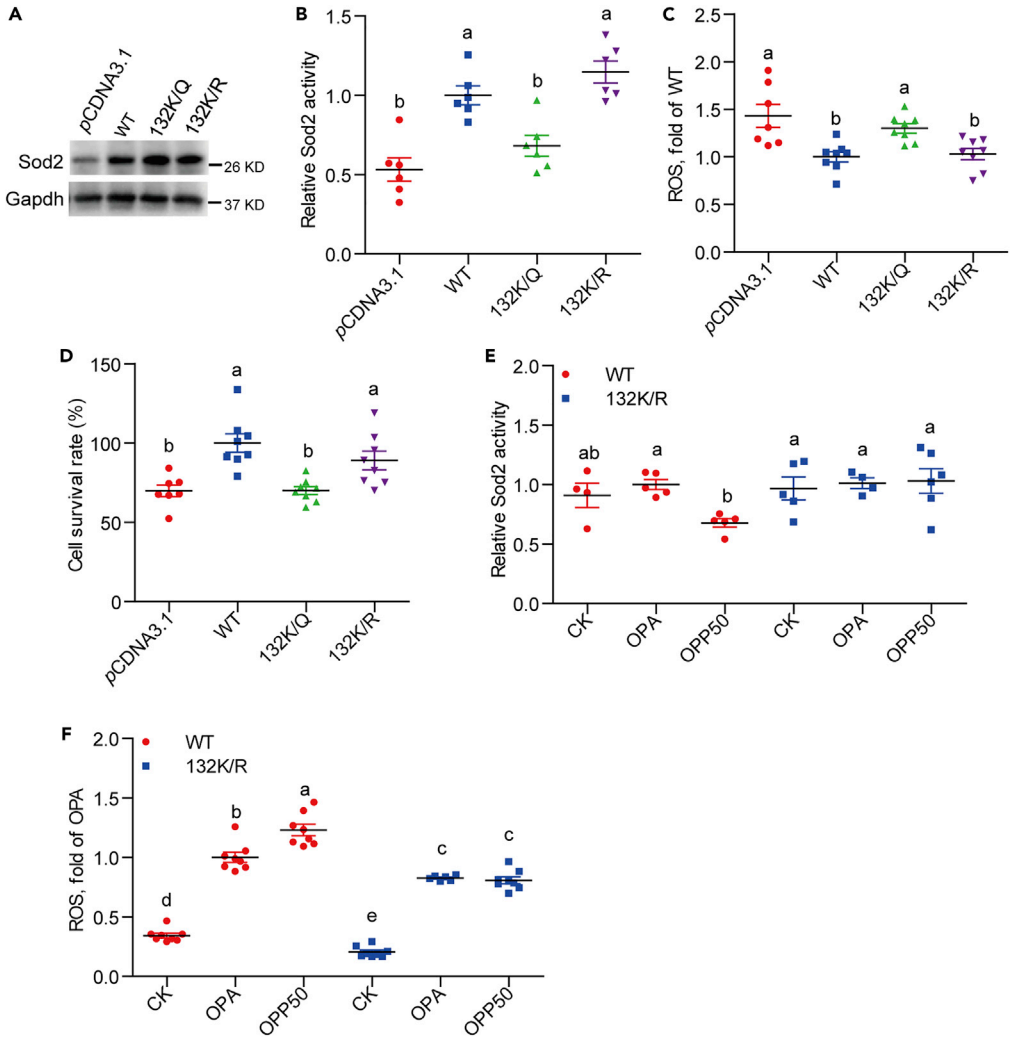

Figure 5. Sod2 propionylation at 132 lysine site accounts for cellular ROS increase

(A) A representative western blotting showing that overexpression of WT Sod2 and Sod2 K132R/Q compensated Sod2 level in ZF4 cells (with endogenous Sod2 knockdown).

(B–D) (B) Sod2 activity, (C) ROS level, and (D) cell survival rate in ZF4 cells transfecting with WT Sod2 or Sod2 K132R/Q mutants (with endogenous Sod2 knockdown) (n = 6–8).

(E) Sod2 activity and (F) ROS level in ZF4 cells treated with OPA or OPP (50 mM propionate), which were transfected with WT Sod2 and Sod2 K132R in advance (without Sod2 knockdown) (n = 4–8).

Values are means ± SEM. Means without a common letter are significantly different ($p < 0.05$). Duncan's test. CK, 5% BSA. See also Figures S5 and S6.

the HFSP0.5 with or without LA. The results showed that the number of Proteobacteria and *Plesiomonas* were significantly reduced when zebrafish were fed the HFSP0.5 supplemented LA as compared with the HFSP0.5 only (Figures 7F and 7G). Moreover, the ROS accumulation in intestine was significantly reduced by LA supplementation (Figure 7H). These results indicate that oxidative stress induced by HFSP0.5 may elevate the abundance of Proteobacteria and alter the composition of gut microbiota.

We observed that ROS in gut content from HFSP0.5 zebrafish was 56.7% higher than that in HFD-fed zebrafish (Figure 7I). Consistently, the ROS accumulation in the gut content was significantly reduced when the HFSP0.5 was supplemented with LA (Figure 7J). Here, the probe dichlorofluorescin (DCFH-DA) also gave the same fluorescence pattern in germ-free (GF) zebrafish fed HFD and HFSP0.5 (Figure 7K). Similarly, the ROS level in the medium of ZF4 cells treated with OPP50 for 24 h was 19.0% higher than that in OPA-treated cells (Figure 7L). However, *in vitro* cultured gut microbiota derived from HFSP0.5-fed zebrafish generated

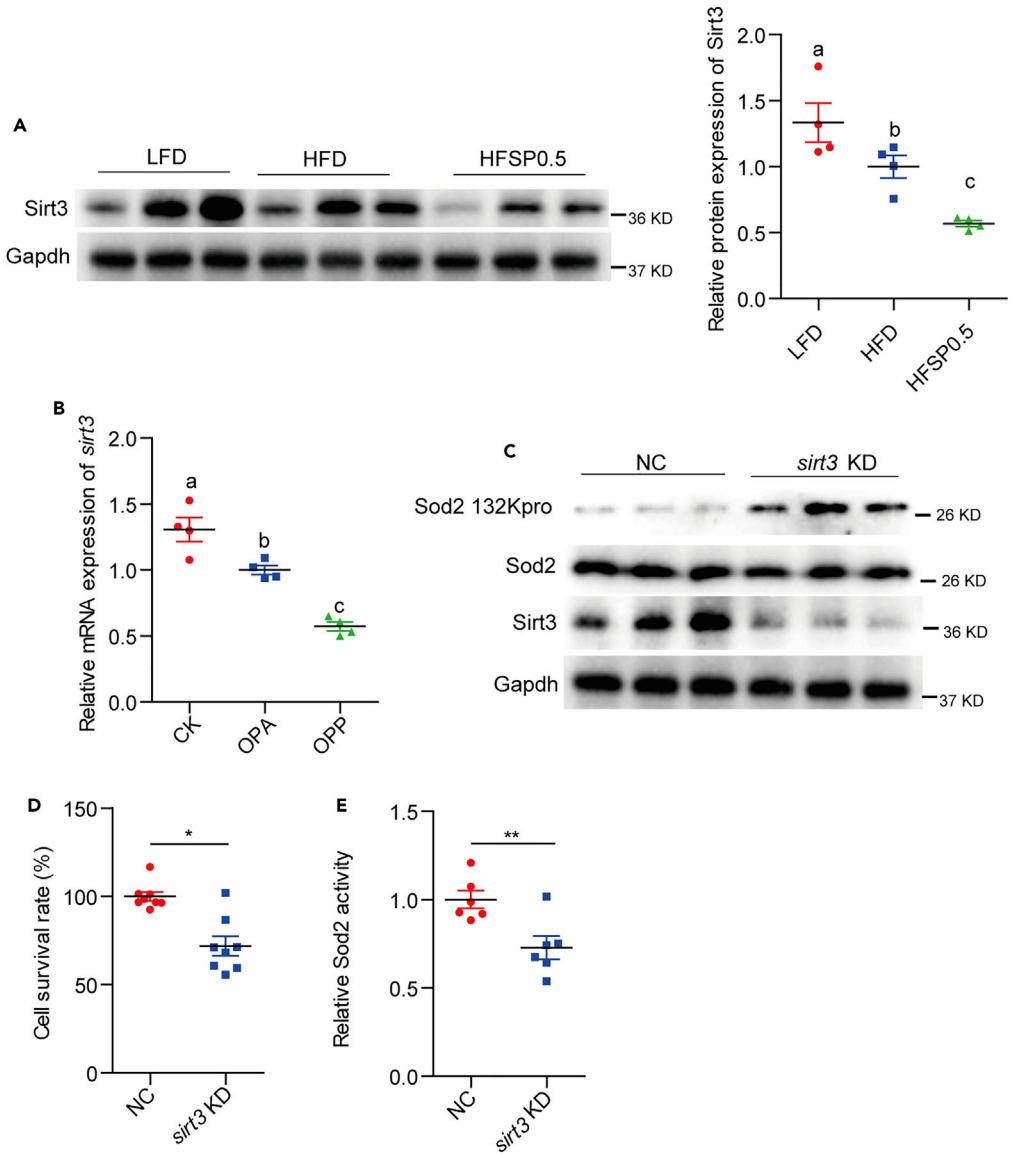

Figure 6. Inhibition of Sirt3 promotes Sod2 propionylation

(A) A representative western blotting showing Sirt3 expression and quantification of intestinal Sirt3 protein level in zebrafish fed LFD, HFD, or HFSP0.5 for 2 weeks (n = 4).

(B) The mRNA expression of *sirt3* in ZF4 cells treated with OPA or OPP50 for 24 h (n = 4).

(C) A representative western blotting showing the propionylation of Sod2 at the 132 lysine site in ZF4 cells upon *sirt3* knockdown.

(D) Cell survival rate in ZF4 cells with *sirt3* knockdown (n = 8).

(E) Sod2 activity in ZF4 cells with *sirt3* knockdown (n = 6).

Values are mean ± SEM. A and B were analyzed by Duncan's test, and means without a common letter are significantly different ($p < 0.05$). D and E were analyzed by Student's t test, *, $p < 0.05$, **, $p < 0.01$.

See also Figures S7 and S8.

similar ROS level to those fed HFD at 24 h (Figure 7M) and decreased at 48 h (Figure 7N). These results indicate that intestinal oxidative stress is derived from the intestinal tissue rather than from the microbiota. This appears to form an oxidative microenvironment in gut, leading to altered microbiota.

To further investigate the role of microbiota, we transferred gut microbiota from zebrafish fed LFD, HFD, and HFSP0.5 into GF zebrafish and assayed for ROS and caspase activity. The gut microbiota from

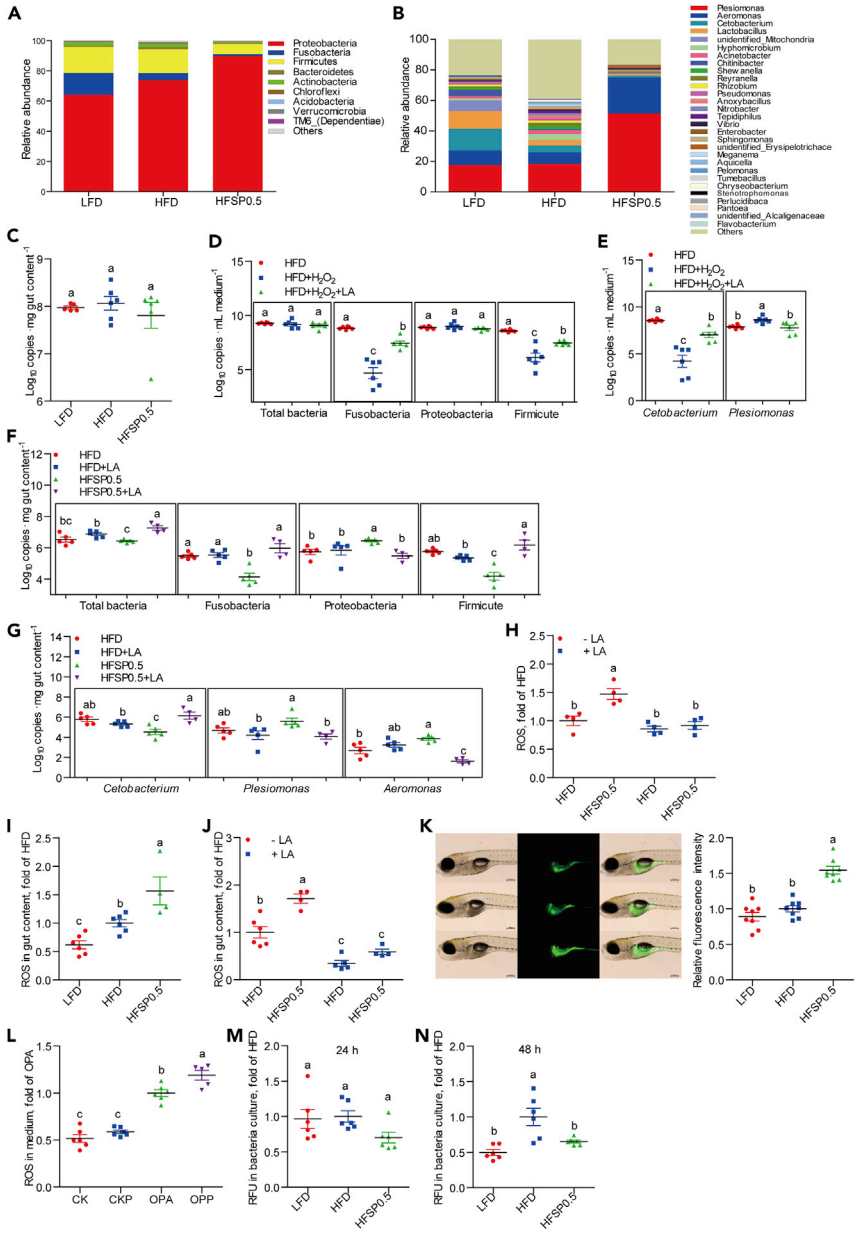

Figure 7. Alteration of gut microbiota is linked to intestinal oxidative stress induced by propionate supplementation in HFD

(A) The composition of gut microbiota at phylum level in 1-month-old zebrafish fed the LFD, HFD, or HFSP0.5 (n = 6).

(B) The composition of gut microbiota at genus level in 1-month-old zebrafish fed the LFD, HFD, or HFSP0.5 (n = 6).

(C) The number of total bacteria in gut content collected from 1-month-old zebrafish fed the LFD, HFD, or HFSP0.5 (Log_{10} 16S *r*DNA gene copies · mg gut content^{-1}) (n = 6).

(D) The number of total bacteria, Fusobacteria, Proteobacteria, and Firmicutes after incubation in GAM with or without H_2O_2 for 48 h (Log_{10} 16S *r*DNA gene copies · mL medium^{-1}) (n = 6).

(E) The number of *Cetobacterium* and *Plesiomonas* after incubation in GAM with or without H_2O_2 for 48 h (n = 6).

(F) The number of total bacteria, Fusobacteria, Proteobacteria, and Firmicutes in gut content collected from 1-month-old zebrafish fed HFSP0.5 with or without supplementation of LA (Log_{10} 16S *r*DNA gene copies · mg gut content^{-1}) (n = 4–5).

(G) The numbers of *Cetobacterium*, *Plesiomonas*, and *Aeromonas* in gut content collected from 1-month-old zebrafish fed HFSP0.5 with or without supplementation of LA (Log_{10} 16S *r*DNA gene copies · mg gut content^{-1}) (n = 4–5).

(H) ROS level in the intestine collected from zebrafish fed the HFD or HFSP0.5 supplemented with LA (n = 4).

(I) ROS level in the gut content collected from zebrafish fed the LFD, HFD, or HFSP0.5 (n = 4–6).

(J) ROS level in gut contents collected from zebrafish fed the HFD or HFSP0.5 supplemented with LA (n = 4–6).

Figure 7. *Continued*

(K) ROS pattern in GF zebrafish fed the LFD, HFD, or HFSP0.5 for 1 week. The scale bar, 200 μm (n = 8).

(L) ROS level in the medium of ZF4 cells treated with OPA or OPP (50 mM propionate) for 24 h (n = 6).

(M and N) ROS generated by *in vitro* cultured gut microbiota derived from LFD-, HFD-, or HFSP0.5-fed zebrafish at (M) 24 h and (N) 48 h (n = 6).

Values are means ± SEM. Means without a common letter are significantly different ($p < 0.05$). Duncan's test.

HFSP0.5-fed zebrafish induced significant elevation of ROS (Figure 8A) and higher caspase-9, caspase-6, and caspase-3 activities as compared with that from HFD-fed zebrafish (Figures 8B–8D). These results indicate that gut microbiota from HFSP0.5-fed zebrafish can activate the mitochondrial death pathway. Gut microbiota from zebrafish fed HFSP0.5 did lead to a moderate, but non-significant, increase in Sirt3 expression (Figure 8E). These results suggest that the role of gut microbiota might be independent of Sirt3.

DISCUSSION

In this study, we conclude that dietary propionate induces oxidative stress and consequent intestinal damage in zebrafish when fed HFD. These damages appeared to be attributed to posttranslational propionylation of the mitochondrial antioxidant enzyme Sod2 and reduced expression of Sirt3, which could function as a de-propionylation agent.

Oxidative stress and mitochondrial abnormality are associated with impaired intestinal health. For instance, they have important pathogenetic implications for inflammatory bowel disease (IBD) (Palucka, 2007; Novak and Mollen, 2015). The gastrointestinal (GI) tract injury effect of nonsteroidal anti-inflammatory drugs (NSAID) is associated with disruption of mitochondrial structure and function (Rafi, 1998; Somasundaram et al., 1997; Kyle, 2014), whereas antioxidant drugs, such as sulfasalazine, are known to have beneficial effects in the treatment of IBD (Bhattacharyya et al., 2014). Oxidative stress is caused by ROS accumulation due to an imbalance in ROS production and removal. Increased ROS production will result in mitochondrial dysfunction (Wei et al., 1998; Duchen, 2004; Pieczenik and Neustadt, 2007). SOD2 is the primary mitochondrial matrix-located enzyme for ROS clearance (Spitz and Oberley, 1989; Zelko et al., 2002). Deficiency of SOD2 activity will impair antioxidant defense and increase oxidative stress, eventually leading to mitochondrial dysfunction (Ramachandran et al., 2011). SOD1, another dismutase, will also remove ROS, but it localizes to the cytoplasm and the intermembrane space of the mitochondria (Fukai and Ushio-Fukai, 2011). SOD2 is more important to prevent oxidative damage than SOD1 (Fukui and Zhu, 2010; Matzuk et al., 1998; Asimakis et al., 2002). In this study, supplementing propionate to HFD increased ROS production and reduced antioxidant capability and Sod2 activity. Moreover, an SOD mimic, 4-hydroxy-TEMPO, relieved the intestinal damage induced by HFSP0.5. These results confirmed that the intestinal damage induced by HFSP0.5 is, at least in part, mediated by oxidative stress resulting from Sod2 inactivation.

Dietary propionate supplementation leads to intestinal Sod2 propionylation at K132. Propionylation of Sod2 was also verified in ZF4 cells treated with OPP and in Sod2 purified from HEK293 cells. *In vitro* incubation with propionyl-CoA leads to propionylation of his-tagged Sod2, suggesting that Sod2 propionylation was mediated by propionyl-CoA, which can be generated from propionate (Schonfeld and Wojtczak, 2016). Decreased transcription of Pcc subunits in both HFD and HFSP0.5 groups reflects blocked propionyl-CoA metabolism, as PCC is the essential enzyme for catalyzing the carboxylation of propionyl-CoA to methylmalonyl-CoA, which ultimately enters the succinyl-CoA pool and the TCA cycle (Wongkittichote et al., 2017; Xu et al., 2018). Therefore, the inhibitory effect of HFD on *pcc* subunit expression may interrupt propionyl-CoA metabolism and increase the local concentration of propionyl-CoA in mitochondria, and this could reduce the tolerance of intestine tissue or cells to exogenous propionate.

Recent studies have shown that PTM of SOD2, such as acetylation at 53, 68, 89, 122, and 130 lysine (Qiu et al., 2010; Tao et al., 2010; Lu et al., 2015; Zhang et al., 2016), negatively regulates its antioxidant activity (Qiu et al., 2010; Tao et al., 2010). According to the alignment of amino acid sequences, the 132 lysine of zebrafish Sod2 (EMBL no. AY195857) is aligned to the 130 lysine of SOD2 in mice (AK002534), rats (BC070913), and humans (M36693) (Lin et al., 2009). Lysine propionylation is chemically similar to acetylation, but the extra methylene-group makes the modification bulkier and more hydrophobic (Bheda et al., 2011). The consequence of such modifications was convincingly demonstrated when the Sod2 activity was increased by the exchange of 132 lysine with arginine (to mimic the de-propionylated state) and reduced by the exchange of 132 lysine with glutamine (to mimic propionylation). Sod2 K132/R mutant can also prevent

Table 2. The predominant gut bacterial phylum in zebrafish fed the LFD, HFD, or HFSP0.5 for 4 weeks based on V3–V4 sequences

Phylum (%)	LFD	HFD	HFSP0.5
Proteobacteria	64.1c±5.9^{b}	73.8 ± 3.1^{b}	89.7 ± 1.8^{a}
Fusobacteria	14.5 ± 3.8^{a}	4.7 ± 1.9^{b}	1.3 ± 0.5^{b}
Firmicutes	17.3 ± 3.5^{a}	15.9 ± 2.7^{a}	6.8 ± 1.3^{b}
Bacteroidetes	0.6 ± 0.2^{a}	1.3 ± 0.6^{a}	0.6 ± 0.2a
Actinobacteria	2.5 ± 0.6^{a}	2.3 ± 0.5^{a}	1.0 ± 0.4^{a}

Values are expressed as the mean ± SEM, n = 6 biological replicates. Means marked with different letters represent statistically significant results ($p < 0.05$), whereas the common letter corresponds to results with no statistically significant differences. Duncan's test.

OPP-induced Sod2 inactivation and ROS accumulation. This shows that K132 is the main propionylated site that accounts for reduced Sod2 activity when exposed to high levels of propionyl-CoA concentration derived from exogenous propionate.

HFD and propionate-induced Sod2 K132 propionylation is accompanied by reduced Sirt3 expression in the intestine of zebrafish, as well as in ZF4 cells treated with OPP. SIRT3 has been suggested to possess de-propionylation activity. For example, the propionyl-lysine modification in propionyl-CoA synthetase introduced by bacterial Gcn-5-related N-acetyltransferase enzymes can be removed by human SIRT3 (Garrity et al., 2007). Moreover, the absence of SIRT3 will lead to a higher propionyl-lysine levels in mouse lenses (Nahomi et al., 2020). In this study, we showed that *sirt3* knockdown increased propionylation of Sod2 at K132 and inhibited its antioxidant activity. This supports the hypothesis that Sirt3 participates in the regulation of Sod2 de-propionylation. Peroxisome-proliferator-activated receptor γ coactivator 1 α (PGC1a) is one of the few known regulators of SIRT3. It will induce SIRT3 expression by binding the ERR-binding element in the promoter region (Kong et al., 2010). The reported transcriptional repressors of SIRT3 include poly (ADP-ribose) polymerase 1 (PARP1) and transcriptional cofactor receptor-interacting protein 140 (RIP140), both of which contribute to oxidative stress and mitochondrial dysfunction (Yoon and Kim, 2016; Kim et al., 2020). In this study, the expression of *pgc1α* and *err* in zebrafish intestine and ZF4 cells showed no significant alteration in response to HFSP0.5 and OPP (50 mM) treatment (data not shown), suggesting that the reduction of *sirt3* expression might be mediated by its transcriptional repressors. Further studies are needed to clarify these regulations of *sirt3* expression in zebrafish fed HFD and propionate.

There is accumulating evidence demonstrating intricate relationships between host oxidative stress and gut microbiota (Qiao et al., 2013; Million et al., 2016). To some extent this probably reflects different tolerances to oxidative stress among anaerobic and aerotolerant bacteria (Liu et al., 2021), although other explanations may also be possible. In this study, we have shown that propionate supplementation to HFD leads to altered gut microbiota with an enrichment of Proteobacteria and *Plesiomonas*. We also conclusively showed that both conventional and GF zebrafish fed HFSP0.5 had increased luminal ROS production, which was confirmed with observations of elevated ROS level in the medium of ZF4 cells treated with OPP. Furthermore, *in vitro* and *in vivo* results showed that the alteration of gut microbiota was attributable to intestinal oxidative stress induced by propionate supplementation to HFD. The detailed mechanisms underlying the relationship between intestinal oxidative stress and gut microbiota remains to be elucidated. It is however quite clear that intestinal oxidative stress induced by exogenous propionate will alter luminal oxidative microenvironment and the gut microbiota.

In the present study, we used gut microbiota transfer to investigate the role of gut microbiota on zebrafish health. We found that transplanting microbiota from HFSP0.5-fed zebrafish to GF zebrafish led to increased ROS accumulation and activation of mitochondrial death pathway. Gut microbiota can stimulate mitochondrial production of ROS via release of various microbiota-associated molecular patterns (MAMPs), including lipopolysaccharides (LPS), flagellin, lipoteichoic acid, lipoprotein, or other toxins (Saint-Georges-Chaumet and Edeas, 2016). These MAMPs are recognized by the pattern recognition receptor (PRR) system in the host cell, which in turn induces ROS production via classical TLR and NLR pathways (Saint-Georges-Chaumet and Edeas, 2016; Emre and Nubel, 2010). Therefore, the alteration in microbiota structure might promote ROS production due to differential microbe-associated molecular patterns

Table 3. The predominant gut bacterial genus in zebrafish fed the LFD, HFD, or HFSP0.5 for 4 weeks based on V3–V4 sequences

Genus (%)	LFD	HFD	HFSP0.5
Plesiomonas	17.5 ± 6.9^{b}	18.3 ± 6.9^{b}	51.4 ± 7.2^{a}
Aeromonas	9.6 ± 2.4^{a}	7.6 ± 2.5^{a}	23.5 ± 2.6^{a}
Cetobacterium	14.3 ± 3.8^{a}	4.6 ± 4.1^{b}	1.2 ± 4.2^{b}
Lactobacillus	11.5 ± 2.7^{a}	3.2 ± 3.3^{b}	0.6 ± 3. 7^{b}
Hyphomicrobium	1.3 ± 0.3^{b}	4.0 ± 0.3^{a}	0.4 ± 0.4^{b}
Acinetobacter	1.6 ± 0.9^{ab}	2.6 ± 0.4^{a}	0.8 ± 0.1^{b}
Chitinibacter	4.3 ± 4.0^{a}	0.5 ± 4.0^{a}	0.1 ± 0.1^{a}

Values are expressed as the mean ± SEM, n = 6 biological replicates. Means marked with different letters represent statistically significant results ($p < 0.05$), whereas the common letter corresponds to results with no statistically significant differences. Duncan's test.

(MAMPs)-PRR signaling. Further studies are needed to identify the role of specific bacteria-deprived MAMPs associated with HFSP0.5-microbiota in promoting host ROS production.

Apart from Sod2, lysine propionylation was also observed in other proteins based on the global lysine propionylation analysis (Figure S4; Tables S3 and S4). The first global survey of lysine propionylation has been reported in *Cyanobacteria* (Yang et al., 2019). To our knowledge, our work was the first global propionylome analysis conducted in animals. The bioinformatics results showed that proteins involved in oxidative phosphorylation (OXPHOS) and ATP synthesis were enriched among the propionylated proteins in the intestine of HFSP0.5-fed zebrafish; this also appeared to be the case with proteins (KEEG pathway) of the TCA cycle. Among the proteins in TCA cycle, malate dehydrogenase 2 (Mdh2) and citrate synthase (Cs) were found to have a complex association with other mitochondrial proteins. This association may indicate other potential regulatory roles of lysine propionylation in mitochondrial metabolism that would act through modulating Mdh2 and Cs activity. These and other roles of global lysine propionylation on mitochondrial energy metabolism deserves further studies.

In propionic acidemia (PA), a human metabolic disorder, the accumulation of propionyl-CoA results in mitochondrial dysfunction and oxidative stress (de Keyzer et al., 2009; Gallego-Villar et al., 2013, 2016). Although studies suggest a role of protein propionylation and oxidative stress in the pathological mechanism of PA, information on possible relationships between mitochondrial protein propionylation and oxidative stress is lacking. Our results identified propionylated Sod2 as one candidate that can cause oxidative stress. It is not unlikely that a similar mechanism may apply to PA pathogenesis. More importantly, propionate is a widely used feed preservative. Our findings clearly indicate potential health hazard of supplementing dietary propionate to fish when combined with HFD formulations, which are very common for fish culture. Moreover, the results also suggest a novel and important aspect of propionate safety in the context of HFD for humans, especially for those with pre-existing intestinal health issues. These issues deserve further investigation in mammalian models.

Limitations of study

In this study, our data demonstrate that propionate supplementation to HFD induces intestinal oxidative stress via Sod2 K132 propionylation. The Sod2 propionylation is associated with decreased expression of Pcc and Sirt3, which leads to increased propionyl-CoA level and reduced depropionylation activity, respectively. However, the underlying mechanisms are not clear and deserves further investigation. Furthermore, our findings suggest potential risk of propionate as feed additive but cannot directly translate to food additive for humans, which requires evaluation in mammal models.

STAR★METHODS

Detailed methods are provided in the online version of this paper and include the following:

- KEY RESOURCES TABLE
- RESOURCE AVAILABILITY
  - Lead contact

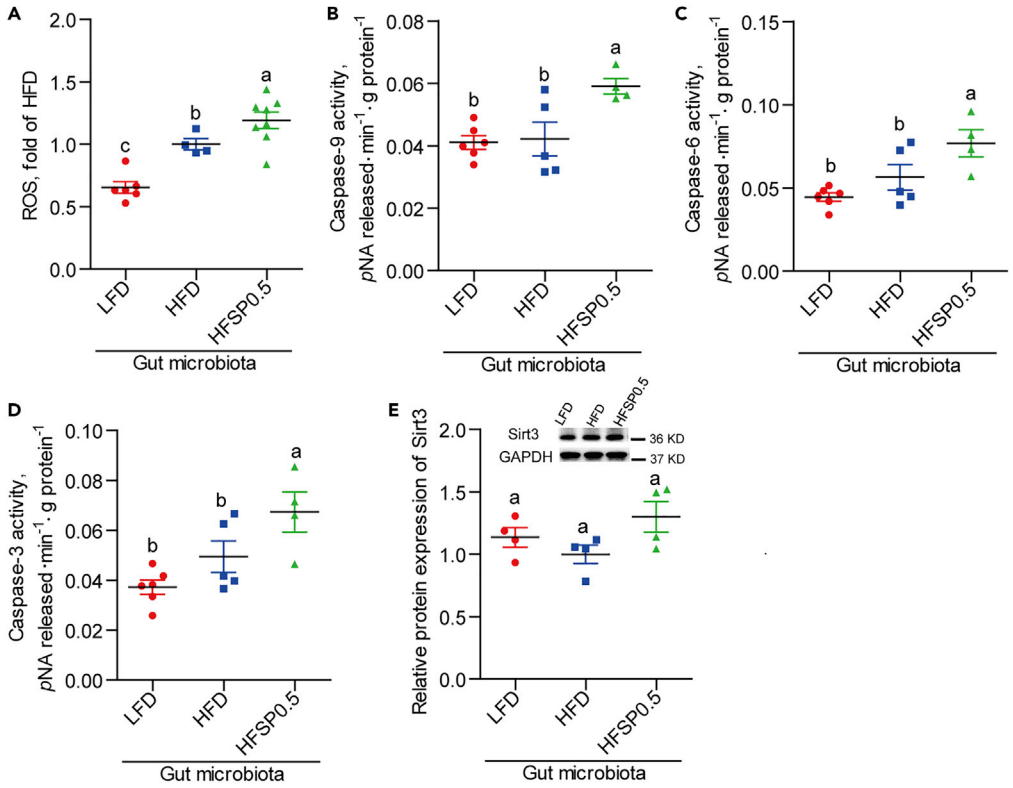

Figure 8. Gut microbiota indirectly activate mitochondrial death pathway

(A) The ROS level in GF zebrafish colonized with gut microbiota from 1-month-old zebrafish fed the LFD, HFD, or HFSP0.5 (n = 4–8).

(B–D) (B) Caspase-9, (C) caspase-6, and (D) caspase-3 activities in GF zebrafish colonized with gut microbiota from 1-month-old zebrafish fed the LFD, HFD, or HFSP0.5 (n = 4–6).

(E) Quantification of Sirt3 protein level in GF zebrafish transferred with gut microbiota from 1-month-old zebrafish fed the LFD, HFD, or HFSP0.5 (n = 4). Values are means ± SEM. Means without a common letter are significantly different ($p < 0.05$). Duncan's test.

- Materials availability
- Data and code availability
- EXPERIMENTAL MODEL AND SUBJECT DETAILS
  - Animals and diets
  - ZF4 cell line
- METHOD DETAILS
  - *Aeromonas veronii* challenge assay
  - Serum endotoxin assay
  - Examination of intestinal histopathology
  - Detection of caspase activity
  - ROS detection in intestinal mitochondria
  - Detection of oxidative parameters
  - Evaluation of total antioxidant capacity
  - Evaluation of antioxidant enzyme activity
  - Intraperitoneal injection of 4-hydroxy-TEMPO
  - Identification of lysine propionylated sites by HPLC-MS/MS
  - Cell viability analysis
  - Cell apoptosis analysis
  - Cellular ROS determination
  - Determination of ROS in gut content and cell medium
  - Gene silencing with *si*RNA

- *In vitro* propionylation assay
- Plasmid construction and transfection
- Gut microbiota analysis
- Germ-free zebrafish generation and treatment
- Detection of ROS in whole zebrafish larvae
- *In vitro* culture of gut microbiota and quantification
- Detection of ROS in gut microbiota medium
- Western blotting
- Total RNA extraction, reverse transcription, and *q*PCR

● QUANTIFICATION AND STATISTICAL ANALYSIS

SUPPLEMENTAL INFORMATION

Supplemental information can be found online at https://doi.org/10.1016/j.isci.2021.102515.

ACKNOWLEDGMENTS

This work was supported by the National Natural Science Foundation of China (NSFC 31925038, 32061133004) and the National Key R&D Program of China (2018YFD0900400). The authors thank Prof. Nicholas Clarke for linguistic proof reading.

AUTHOR CONTRIBUTIONS

Z.Zhou. designed and supervised the research. Q.D. and C.R. wrote the paper. Z.Zhou. and C.R. gave conceptual advice for the paper. J.L.C., E.R., and R.E.O. reviewed and helped to revise the manuscript. Q.D. performed experiments and acquired data. Z.Zhang. and Y.L. assisted in the *q*PCR, western blot, gut microbiota analysis, and *si*RNA knockdown experiments. H.L. and Q.H. participated in zebrafish husbandry and sampling. C.R., Y.Y., and Z.Zhang. co-analyzed and discussed the results. All authors read and approved the final manuscript.

DECLARATION OF INTERESTS

The authors declare no competing interests.

Received: January 15, 2021
Revised: March 17, 2021
Accepted: May 3, 2021
Published: June 25, 2021

REFERENCES

Asimakis, G.K., Lick, S., and Patterson, C. (2002). Postischemic recovery of contractile function is impaired in SOD2(+/-) but not SOD1(+/-) mouse hearts. Circulation *105*, 981–986.

Bhattacharyya, A., Chattopadhyay, R., Mitra, S., and Crowe, S.E. (2014). Oxidative stress: an essential factor in the pathogenesis of gastrointestinal mucosal diseases. Physiol. Rev. *94*, 329–354.

Bhatti, J.S., Bhatti, G.K., and Reddy, P.H. (2017). Mitochondrial dysfunction and oxidative stress in metabolic disorders - a step towards mitochondria based therapeutic strategies. Biochim. Biophys. Acta Mol. Basis Dis. *1863*, 1066–1077.

Bheda, P., Wang, J.T., Escalante-Semerena, J.C., and Wolberger, C. (2011). Structure of Sir2Tm bound to a propionylated peptide. Protein Sci. *20*, 131–139.

Chen, Y., Sprung, R., Tang, Y., Ball, H., Sangras, B., Kim, S.C., Falck, J.R., Peng, J., Gu, W., and Zhao, Y. (2007). Lysine propionylation and butyrylation are novel post-translational modifications in histones. Mol. Cell Proteomics *6*, 812–819.

Cheng, Z., Tang, Y., Chen, Y., Kim, S., Liu, H., Li, S.S., Gu, W., and Zhao, Y. (2009). Molecular characterization of propionyllysines in non-histone proteins. Mol. Cell Proteomics *8*, 45–52.

Circu, M.L., and Aw, T.Y. (2012). Intestinal redox biology and oxidative stress. Semin. Cell Dev. Biol. *23*, 729–737.

de Keyzer, Y., Valayannopoulos, V., Benoist, J.F., Batteux, F., Lacaille, F., Hubert, L., Chretien, D., Chadefeaux-Vekemans, B., Niaudet, P., Touati, G., et al. (2009). Multiple OXPHOS deficiency in the liver, kidney, heart, and skeletal muscle of patients with methylmalonic aciduria and propionic aciduria. Pediatr. Res. *66*, 91–95.

Driever, W., and Rangini, Z. (1993). Characterization of a cell line derived from zebrafish (Brachydanio rerio) embryos. In Vitro Cell. Dev. Biol. Anim. *29A*, 749–754.

Du, S.F., Wang, H.J., Zhang, B., Zhai, F.Y., and Popkin, B.M. (2014). China in the period of transition from scarcity and extensive undernutrition to emerging nutrition-related non-communicable diseases, 1949-1992. Obes. Rev. *15*, 8–15.

Duchen, M.R. (2004). Mitochondria in health and disease: perspectives on a new mitochondrial biology. Mol. Aspects Med. *25*, 365–451.

Edgar, R.C. (2013). UPARSE: highly accurate OTU sequences from microbial amplicon reads. Nat. Methods *10*, 996–+.

Edgar, R.C. (2010). Search and clustering orders of magnitude faster than BLAST. Bioinformatics *26*, 2460–2461.

Emre, Y., and Nubel, T. (2010). Uncoupling protein UCP2: when mitochondrial activity meets immunity. FEBS Lett. *584*, 1437–1442.

Fernandez-Vizarra, E., Fernandez-Silva, P., and Enriquez, J.A. (2006). Isolation of mitochondria from mammalian tissues and cultured Cells. In

Cell Biology: A Laboratory Handbook, J.E. Celis, ed. (Elsevier-Academic Press), pp. 69–77.

Flavin, M., and Ochoa, S. (1957). Metabolism of propionic acid in animal tissues. I. Enzymatic conversion of propionate to succinate. J. Biol. Chem. *229*, 965–979.

Fukai, T., and Ushio-Fukai, M. (2011). Superoxide dismutases: role in redox signaling, vascular function, and diseases. Antioxidants & Redox Signaling *15*, 1583–1606.

Fukui, M., and Zhu, B.T. (2010). Mitochondrial superoxide dismutase SOD2, but not cytosolic SOD1, plays a critical role in protection against glutamate-induced oxidative stress and cell death in HT22 neuronal cells. Free Radic. Biol. Med. *48*, 821–830.

Gallego-Villar, L., Perez-Cerda, C., Perez, B., Abia, D., Ugarte, M., Richard, E., and Desviat, L.R. (2013). Functional characterization of novel genotypes and cellular oxidative stress studies in propionic acidemia. J. Inherit. Metab. Dis. *36*, 731–740.

Gallego-Villar, L., Rivera-Barahona, A., Cuevas-Martin, C., Guenzel, A., Perez, B., Barry, M.A., Murphy, M.P., Logan, A., Gonzalez-Quintana, A., Martin, M.A., et al. (2016). In vivo evidence of mitochondrial dysfunction and altered redox homeostasis in a genetic mouse model of propionic acidemia: implications for the pathophysiology of this disorder. Free Radic. Biol. Med. *96*, 1–12.

Garrity, J., Gardner, J.G., Hawse, W., Wolberger, C., and Escalante-Semerena, J.C. (2007). N-Lysine propionylation controls the activity of propionyl-CoA synthetase. J. Biol. Chem. *282*, 30239–30245.

Kebede, A.F., Nieborak, A., Shahidian, L.Z., Le Gras, S., Richter, F., Gomez, D.A., Baltissen, M.P., Meszaros, G., Magliarelli, H.D., Taudt, A., et al. (2017). Histone propionylation is a mark of active chromatin. Nat. Struct. Mol. Biol. *24*, 1048–+.

Kim, S., Piao, S., Lee, I., Nagar, H., Choi, S.J., Shin, N., Kim, D.W., Shong, M., Jeon, B.H., and Kim, C.S. (2020). CR6 interacting factor 1 deficiency induces premature senescence via SIRT3 inhibition in endothelial cells. Free Radic. Biol. Med. *150*, 161–171.

Koh, A., De Vadder, F., Kovatcheva-Datchary, P., and Backhed, F. (2016). From dietary fiber to host physiology: short-chain fatty acids as key bacterial metabolites. Cell *165*, 1332–1345.

Kyle, S.S. (2014). Mechanisms of NSAID-induced small intestinal injury: role of bacterial beta-glucuronidase, the microbiome, and mitochondria. Microbiol. Immunol. *28*, 975–986.

Kong, X.X., Wang, R., Xue, Y., Liu, X.J., Zhang, H.B., Chen, Y., Fang, F., and Chang, Y.S. (2010). Sirtuin 3, a new target of PGC-1 alpha, plays an important role in the suppression of ROS and mitochondrial biogenesis. PLoS One *5*, e11707.

Lackmann, C., Santos, M., Rainieri, S., Barranco, A., Hollert, H., Spirhanzlova, P., Velki, M., and Seiler, T.B. (2018). Novel procedures for whole organism detection and quantification of fluorescence as a measurement for oxidative stress in zebrafish (*Danio rerio*) larvae. Chemosphere *197*, 200–209.

Lagerwaard, B., Pougovkina, O., Bekebrede, A.F., te Brinke, H., Wanders, R.J.A., Nieuwenhuizen, A.G., Keijer, J., and de Boer, V.C.J. (2020). Increased protein propionylation contributes to mitochondrial dysfunction in liver cells and fibroblasts, but not in myotubes. J. Inherit. Metab. Dis. *44*, 438–449.

Lin, C.T., Tseng, W.C., Hsiao, N.W., Chang, H.H., and Ken, C.F. (2009). Characterization, molecular modelling and developmental expression of zebrafish manganese superoxide dismutase. Fish Shellfish Immunol. *27*, 318–324.

Liu, B., Lin, Y.H., Darwanto, A., Song, X.H., Xu, G.L., and Zhang, K.L. (2009). Identification and characterization of propionylation at histone H3 lysine 23 in mammalian cells. J. Biol. Chem. *284*, 32288–32295.

Liu, S., Dai, J., Lan, X., Fan, B., Dong, T., Zhang, Y., and Han, M. (2021). Intestinal bacteria are potential biomarkers and therapeutic targets for gastric cancer. Microb. Pathog. *151*, 104747.

Liu, X., Zhu, C.C., Zha, H.Y., Tang, J.H., Rong, F.J., Chen, X.Y., Fan, S.J., Xu, C.X., Du, J., Zhu, J.J., et al. (2020). SIRT5 impairs aggregation and activation of the signaling adaptor MAVS through catalyzing lysine desuccinylation. EMBO J. *39*, e103285.

Lu, J.Q., Cheng, K.Y., Zhang, B., Xu, H., Cao, Y.Z., Guo, F., Feng, X.D., and Xia, Q. (2015). Novel mechanisms for superoxide-scavenging activity of human manganese superoxide dismutase determined by the K68 key acetylation site. Free Radic. Biol. Med. *85*, 114–126.

Maidak, B.L., Olsen, G.J., Larsen, N., Overbeek, R., McCaughey, M.J., and Woese, C.R. (1997). The RDP (ribosomal database Project). Nucleic Acids Res. *25*, 109–110.

Matsuishi, T., Stumpf, D.A., Seliem, M., Eguren, L.A., and Chrislip, K. (1991). Propionate mitochondrial toxicity in liver and skeletal muscle: acyl CoA levels. Biochem. Med. Metab. Biol. *45*, 244–253.

Matzuk, M.M., Dionne, L., Guo, Q.X., Kumar, T.R., and Lebovitz, R.M. (1998). Ovarian function in superoxide dismutase 1 and 2 knockout mice. Endocrinology *139*, 4008–4011.

Million, M., Tidjani Alou, M., Khelaifia, S., Bachar, D., Lagier, J.C., Dione, N., Brah, S., Hugon, P., Lombard, V., Armougom, F., et al. (2016). Increased gut redox and Depletion of anaerobic and methanogenic prokaryotes in severe acute malnutrition. Sci. Rep. *6*, 26051.

Nahomi, R.B., Nandi, S.K., Rakete, S., Michel, C., Fritz, K.S., and Nagaraj, R.H. (2020). Lysine malonylation and propionylation are prevalent in human lens proteins. Exp. Eye Res. *190*, 107864.

Novak, E.A., and Mollen, K.P. (2015). Mitochondrial dysfunction in inflammatory bowel disease. Front. Cell. Dev. Biol. *3*, 62.

Palucka, T. (2007). Toying with a ridiculous material. Mrs Bull. *32*, 283.

Pieczenik, S.R., and Neustadt, J. (2007). Mitochondrial dysfunction and molecular pathways of disease. Exp. Mol. Pathol. *83*, 84–92.

Qiao, Y., Sun, J., Ding, Y.Y., Le, G.W., and Shi, Y.H. (2013). Alterations of the gut microbiota in high-fat diet mice is strongly linked to oxidative stress. Appl. Microbiol. Biotechnol. *97*, 1689–1697.

Qiu, X.L., Brown, K., Hirschey, M.D., Verdin, E., and Chen, D. (2010). Calorie restriction reduces oxidative stress by SIRT3-mediated SOD2 activation. Cell Metab. *12*, 662–667.

Rafi, S.S. (1998). Studies on the Pathogenesis of NSAID-Induced Damage to the Gastrointestinal Tract with Special Reference to the Mitochondria (ETH), p. 326317.

Ramachandran, A., Lebofsky, M., Weinman, S.A., and Jaeschke, H. (2011). The impact of partial manganese superoxide dismutase (SOD2)-deficiency on mitochondrial oxidant stress, DNA fragmentation and liver injury during acetaminophen hepatotoxicity. Toxicol. Appl. Pharmacol. *251*, 226–233.

Rawls, J.F., Mahowald, M.A., Ley, R.E., and Gordon, J.I. (2006). Reciprocal gut microbiota transplants from zebrafish and mice to germ-free recipients reveal host habitat selection. Cell *127*, 423–433.

Rose, M.D. (2013). Efsa panel on food additives and nutrient sources added to food (ans). EFSA J. *11*, 3234.

Saint-Georges-Chaumet, Y., and Edeas, M. (2016). Microbiota-mitochondria inter-talk: consequence for microbiota-host interaction. Pathog. Dis. *74*, ftv096.

Schonfeld, P., and Wojtczak, L. (2016). Short- and medium-chain fatty acids in energy metabolism: the cellular perspective. J. Lipid Res. *57*, 943–954.

Schwab, M.A., Sauer, S.W., Okun, J.G., Nijtmans, L.G.J., Rodenburg, R.J.T., van den Heuvel, L.P., Drose, S., Brandt, U., Hoffmann, G.F., Ter Laak, H., et al. (2006). Secondary mitochondrial dysfunction in propionic aciduria: a pathogenic role for endogenous mitochondrial toxins. Biochem. J. *398*, 107–112.

Shapawi, R., Ebi, I., Yong, A.S.K., and Ng, W.K. (2014). Optimizing the growth performance of brown-marbled grouper, Epinephelus fuscoguttatus (Forskal), by varying the proportion of dietary protein and lipid levels. Anim. Feed Sci. Technol. *191*, 98–105.

Somasundaram, S., Rafi, S., Hayllar, J., Sigthorsson, G., Jacob, M., Price, A.B., Macpherson, A., Mahmod, T., Scott, D., Wrigglesworth, J.M., and Bjarnason, I. (1997). Mitochondrial damage: a possible mechanism of the "topical" phase of NSAID induced injury to the rat intestine. Gut *41*, 344–353.

Spitz, D.R., and Oberley, L.W. (1989). An assay for superoxide dismutase activity in mammalian tissue homogenates. Anal Biochem. *179*, 8–18.

Starai, V.J., Celic, I., Cole, R.N., Boeke, J.D., and Escalante-Semerena, J.C. (2002). Sir2-dependent activation of acetyl-CoA synthetase by deacetylation of active lysine. Science *298*, 2390–2392.

Tao, R.D., Coleman, M.C., Pennington, J.D., Ozden, O., Park, S.H., Jiang, H.Y., Kim, H.S., Flynn, C.R., Hill, S., McDonald, W.H., et al. (2010). Sirt3-Mediated deacetylation of evolutionarily

conserved lysine 122 regulates MnSOD activity in response to stress. Mol. Cell *40*, 893–904.

Wei, Y.H., Lu, C.Y., Lee, H.C., Pang, C.Y., and Ma, Y.S. (1998). Oxidative damage and mutation to mitochondrial DNA and age-dependent decline of mitochondrial respiratory function. Ann. N Y Acad. Sci. *854*, 155–170.

Wongkittichote, P., Mew, N.A., and Chapman, K.A. (2017). Propionyl-CoA carboxylase - a review. Mol. Genet. Metab. *122*, 145–152.

Xu, J.Y., Xu, Y., Xu, Z., Zhai, L.H., Ye, Y., Zhao, Y.M., Chu, X.H., Tan, M.J., and Ye, B.C. (2018). Protein acylation is a general regulatory mechanism in biosynthetic pathway of acyl-CoA-derived natural products. Cell Chem. Biol. *25*, 984–+.

Yang, M.K., Huang, H., and Ge, F. (2019). Lysine propionylation is a widespread post-translational modification involved in regulation of photosynthesis and metabolism in Cyanobacteria. Int. J. Mol. Sci. *20*, 4792.

Yoon, S.P., and Kim, J. (2016). Poly(ADP-ribose) polymerase 1 contributes to oxidative stress through downregulation of sirtuin 3 during cisplatin nephrotoxicity. Anat. Cell Biol. *49*, 165–176.

Zelko, I.N., Mariani, T.J., and Folz, R.J. (2002). Superoxide dismutase multigene family: a comparison of the CuZn-SOD (SOD1), Mn-SOD (SOD2), and EC-SOD (SOD3) gene structures, evolution, and expression. Free Radic. Biol. Med. *33*, 337–349.

Zeng, X.L., Yang, J.N., Hu, O., Huang, J., Ran, L., Chen, M.T., Zhang, Y., Zhou, X., Zhu, J.D., Zhang, Q.Y., et al. (2019). Dihydromyricetin ameliorates nonalcoholic fatty liver disease by improving mitochondrial respiratory capacity and redox homeostasis through modulation of SIRT3 signaling. Antioxid. Redox Signal. *30*, 163–183.

Zhai, F.Y., Du, S.F., Wang, Z.H., Zhang, J.G., Du, W.W., and Popkin, B.M. (2014). Dynamics of the Chinese diet and the role of urbanicity, 1991-2011. Obes. Rev. *15*, 16–26.

Zhang, K., Chen, Y., Mang, Z.H., and Zhao, Y.M. (2009). Identification and verification of lysine propionylation and butyrylation in yeast core histones using PTMap software. J. Proteome Res. *8*, 900–906.

Zhang, H.H., Ma, X.J., Wu, L.N., Zhao, Y.Y., Zhang, P.Y., Zhang, Y.H., Shao, M.W., Liu, F., Li, F., and Qin, G.J. (2016). Sirtuin-3 (SIRT3) protects pancreatic beta-cells from endoplasmic reticulum (ER) stress-induced apoptosis and dysfunction. Mol. Cell Biochem *420*, 95–106.

Zhang, Z., Ran, C., Ding, Q.W., Liu, H.L., Xie, M.X., Yang, Y.L., Xie, Y.D., Gao, C.C., Zhang, H.L., and Zhou, Z.G. (2019). Ability of prebiotic polysaccharides to activate a HIF1 alpha-antimicrobial peptide axis determines liver injury risk in zebrafish. Commun. Biol. *2*, 274.

STAR★METHODS

KEY RESOURCES TABLE

REAGENT or RESOURCE	SOURCE	IDENTIFIER
Antibodies		
Rabbit polyclonal Anti-Gapdh	Sigma	CAT# SAB2701826;
Rabbit polyclonal Anti-Sod2	GeneTex	CAT#GTX124294; RRID:AB_11174816
Rabbit polyclonal Anti-Sirt3	Sigma	CAT#AV32388; RRID:AB_1856904
Mouse monoclonal Anti-Mtco1	Abcam	CAT#ab14705; RRID:AB_2084810
Rabbit polyclonal Acetyl-Lysine antibody	Cell Signaling Technology	CAT#9441; RRID:AB_331805
Rabbit polyclonal Anti-Sod2 K132pro	This paper	N/A
Bacterial and virus strains		
Aeromonas veronii Hm091	Pearl River Fisheries Research Institute	N/A
Chemicals, peptides, and recombinant proteins		
4-Hydroxy-TEMPO	Sigma	CAT#176141
Protease inhibitor cocktail	Cell Signaling Technology	CAT#5871
AlarmaBlue cell viability reagent	Invitrogen	CAT#DAL1025
Sodium oleate	Sigma	CAT#O7501
Palmitic acid	Sigma	CAT#P5585
Sodium propionate	Sigma	CAT#P1880
DCFH-DA	Beyotime	CAT#S0033S
Propionyl coenzyme A sodium salt	zzstandard	CAT#ZL-21372
PMSF	Beyotime	CAT#ST506
Lipofectamine 3000 transfection reagent	Invitrogen	CAT#L3000008
Lipofectamine RNAiMAX transfection reagent	Invitrogen	CAT#13778
SYBR Green Supermix	TIANGEN	CAT#FP205
Critical commercial assays		
ToxinSensor Chromogenic LAL Endotoxin Assay Kit	Genscript	CAT#L00350
Caspase-9 Activity Assay Kit	Beyotime	CAT#C1158
Fluorometric Intracellular Ros Kit	Sigma	CAT#MAK143
Lipid Peroxidation (MDA) Assay Kit	Sigma	CAT#MAK085
Protein Carbonyl Content Assay Kit	Sigma	CAT#MAK094
Total Antioxidant Capacity Assay Kit	Beyotime	CAT#S0116
CuZn/Mn-SOD Activity Kit	Beyotime	CAT#S0103
Annexin V-FITC Apoptosis Kit	Sigma	CAT#apoaf
QuikChange Site-Directed Mutagenesis Kit	Stratagene	CAT#200523
Deposited data		
Microbiota sequencing data	This paper	BioProject: PRJNA714780
Experimental models: Cell lines		
ZF4: zebrafish embryo	ATCC	CRL-2050
Experimental models: Organisms/strains		
Zebrafish: Tübingen strain	China Zebrafish Resource Center	CZ3

(*Continued on next page*)

Continued

REAGENT or RESOURCE	SOURCE	IDENTIFIER
Oligonucleotides		
*si*RNA	This paper	Table S5
Primers	This paper	Table S6
Recombinant DNA		
Plasmids: *p*CDHA3.1-flag-Sod2, *p*CDHA3.1-flag-Sod2132K/Q and *p*CDHA3.1-flag-Sod2 132K/R	This paper	N/A
Plasmid: *p*CDHA3.1-his-flag-Sod2	This paper	N/A
Software and algorithms		
Guava easyCyte Flow Cytometer software	Merck Millipore, Stafford, VA, USA	N/A
GraphPad Prism 5	GraphPad Software Inc., San Diego, CA, USA	N/A

RESOURCE AVAILABILITY

Lead contact

Further information and requests for resources and reagents should be directed to and will be fulfilled by the lead contact, Zhigang Zhou (email: zhouzhigang03@caas.cn).

Materials availability

Plasmids generated in this study are available from the lead contact upon reasonable request.

Data and code availability

Microbiota sequencing data in this study are available from the National Center for Biotechnology Information (NCBI) under accession number BioProject: PRJNA714780.

EXPERIMENTAL MODEL AND SUBJECT DETAILS

Animals and diets

All experimental and animal care procedures were approved by the Feed Research Institute of the Chinese Academy of Agricultural Sciences Animal Care Committee under the auspices of the China Council for Animal Care (Assurance No. 2016-AF-FRI-CAAS-001). Healthy, uniformly sized 1-month-old zebrafish (Tübingen strain) were divided into eight groups at random and fed the experimental diets (Tables S1 and S2) at the zebrafish facility of the Feed Research Institute of the Chinese Academy of Agricultural Sciences (Beijing, China) twice a day (9:00, 17:00) to apparent satiation for 2 weeks. For the study both sexes were used. During the feeding period, the rearing temperature was 25–28°C, the dissolved oxygen was >6.0 mg/L, the pH was 7.0–7.2, the nitrogen content was <0.50 mg/L, and the nitrogen content (as NO_2) was <0.02 mg/L. All fish were anesthetized with tricaine methanesulfonate (MS222).

ZF4 cell line

The ZF4 cell line was purchased from American Type Culture Collection (Manassas, VA, USA), and cultured according to established protocols (Driever and Rangini, 1993). The medium (DMEM/F12) was obtained from Corning Inc. (New York, USA). Penicillin-Streptomycin solution were purchased from Sigma (St. Louis, MO, USA). Fetal bovine serum was purchased from Corning Inc. (New York, USA). Cells were kept in a cell incubator with 5% CO_2 at 28°C.

METHOD DETAILS

Aeromonas veronii challenge assay

The Aeromonas strain used in this study was *A. veronii* Hm091 isolated by Pearl River Fisheries Research Institute (Guangzhou, China). *A. veronii* Hm091 was grown for 18 h at 37°C in LB medium. Three replicates of 10 zebrafish from each group were infected with Hm091 at 2×10^7 CFU/mL. For challenge, zebrafish were immersed in water containing the pathogen, and mortality was recorded for the 3 days following infection.

Serum endotoxin assay

Serum endotoxin levels were determined using the ToxinSensor Chromogenic LAL Endotoxin Assay Kit (Genscript, Jiangsu Province, China). In brief, serum samples were dispensed into endotoxin-free vials and then consecutively incubated with LAL and chromogenic substrate consecutively. After the reaction was stopped, absorbance of each sample was read at 545 nm. The serum level of endotoxin in adult zebrafish was expressed as endotoxin units per milliliter serum (EU/mL).

Examination of intestinal histopathology

The intestines of zebrafish were rinsed with sterilized PBS, fixed in 4% formalin solution, and embedded in paraffin. For histological analysis, the liver sections were prepared from the paraffin blocks stained with hematoxylin and eosin (H&E). Images were obtained under a microscope (Carl Zeiss) at a 200× magnification.

Detection of caspase activity

The activities of caspase-3, caspase-6, and caspase-9 were determined using an assay kit (Beyotime Biotechnology, Shanghai, China) according to the manufacturer's instructions. The optical density of the reaction product was examined at 405 nm. The enzyme activity is expressed as the rate of *p*-nitroaniline (*p*NA) released from the substrate per gram protein (μmol *p*NA released $min^{-1} \cdot g^{-1}$ protein).

ROS detection in intestinal mitochondria

Intestinal mitochondria were isolated by using a tissue mitochondria isolation kit (Beyotime Biotechnology, Shanghai, China). In brief, fresh intestine was collected from zebrafish and homogenized for 10 times in the isolation buffer using a glass homogenizer. The homogenate was then centrifugated at 1000 g for 10 min. The supernatant was then aspirated and further centrifugated at 11,000 g for 10 min. The precipitation was resuspended in the mitochondria storage buffer. The purity of isolated mitochondria was assessed according to Fernandez-Vizarra et al. (2006) (Figures S9A–S9D). Then isolated mitochondria were incubated with a fluorescent probe provided by the ROS kit (Sigma, USA) for 2 h in a 96-well flat-bottom plate. The fluorescence intensity was measured excitation 490 nm and emission 520 nm. The ROS level was expressed as the fold change compared with the HFD group. Rosup was applied as a positive control (Figure S9E).

Detection of oxidative parameters

Fresh intestine was homogenized in ice-cold MDA lysis buffer and centrifuged at 13,000 g for 10 min to remove insoluble material. Lipid peroxidation was determined by the reaction of malondialdehyde (MDA) with thiobarbituric acid using a lipid peroxidation assay kit according to the manufacturer's instructions (Sigma, USA). In brief, the supernatant was collected and incubated with the TBA solution at 95°C for 60 min to generate MDA-TBA adduct. The optical density of the MDA-TBA adduct was examined at 532 nm. Lipid peroxidation was expressed as MDA content per 100 milligram tissue (nmol · 100 mg $tissue^{-1}$). Oxidation of proteins was determined by the formation of stable dinitrophenyl hydrazine adducts derived from protein carbonyl (PC) groups with 2, 4-dinitrophenylhydrazine using protein carbonyl content assay kit according to the manufacturer's instructions (Sigma, USA). The optical density was examined at 375 nm. Oxidation of proteins was expressed as PC content per milligram protein (nmol · mg $protein^{-1}$).

Evaluation of total antioxidant capacity

Fresh intestine was homogenized in ice-cold PBS to release the antioxidants. The homogenate was then centrifugated at 12,000 g for 5 min and the supernatant collected for subsequent analysis. Total antioxidant capacity (T-AOC) was measured by the production of blue Ferric-tripyridyltriazine (Fe^{2+}-TPTZ) resulting from the reduction of Fe^{3+} TPTZ complex under acidic conditions. The optical density was measured at 593 nm. T-AOC was defined as the production of $FeSO_4$ per gram protein (mmol $FeSO_4$ · g $protein^{-1}$).

Evaluation of antioxidant enzyme activity

Fresh intestine was homogenized in ice-cold PBS, centrifugated at 12,000 g for 5 min, and the supernatant collected for analysis of enzyme activities. The activities of Sod2, glutathione peroxidase (Gpx), and catalase (Cat) were detected using a CuZn/Mn-SOD activity kit, a cellular GPX assay kit, and a catalase (CAT) assay kit (Beyotime Biotechnology, Shanghai, China), respectively. The SOD2 assay included the inhibitors A and B for Cu/Zn SOD (SOD1) (Zeng et al., 2019). Sod2 activity was measured as the inhibition of water soluble tetrazol salt (WST) reduction in a xanthine-xanthine oxidase system. The optical density was measured at 450 nm. Sod2 activity was expressed in units (U) and was the percent inhibition of WST

reduction. The Sod2 activity in the intestine was expressed as the inhibition of WST reduction per milligram protein (U · mg protein^{-1}). Relative Sod2 activity in ZF4 cell and zebrafish larva was expressed as fold change of indicated group. The Gpx activity was analyzed by monitoring NADPH consumption at 340nm using the Gpx detection buffer (3.125 mM NADPH, 3.75 mM GSH and glutathione reductase) and peroxide. The conversion of 1 mmol of NADPH to $NADP^+$ by Gpx per 1 min at 25°C and pH8.0 was set as 1 U. The activity of Gpx was expressed as the conversion rate of NADPH to $NADP^+$ per milligram protein (nmol NADPH conversed · min^{-1} · mg protein^{-1}). The Cat activity was determined by incubating protein in the Cat detection buffer and H_2O_2. At the end of the reaction, the optical density was measured at 520 nm. One U was defined as the decomposition of 1 mmol H_2O_2 at 25°C and pH7.0. The activity of Cat was expressed as the rate of H_2O_2 decomposition per milligram protein (mmol H_2O_2 decomposed · min^{-1} · mg protein^{-1}).

Intraperitoneal injection of 4-hydroxy-TEMPO

After 2-week feeding trial, ten zebrafish from LFD, HFD, and HFSP0.5 groups were respectively divided into two groups: (1) control zebrafish injected intraperitonealy (i.p.) with saline (0.9% NaCl); (2) zebrafish treated i.p. with 4-hydroxy TEMPO dissolved in saline (10 mg · kg b.w.$^{-1}$) every other day. Intestines were collected at the sixth day for H&E staining.

Identification of lysine propionylated sites by HPLC-MS/MS

The intestine was ground by liquid nitrogen into cell powder and then transferred to a 5 mL centrifuge tube. After that, four volumes of lysis buffer (8 M urea, 1% protease inhibitor cocktail, 3 μM trichostation, 50 mM nicotinamide) were added to the cell powder, followed by sonication three times on ice using a high intensity ultrasonic processor. The remaining debris was removed by centrifugation at 12,000 g at 4°C for 10 min. Finally, the supernatant was collected, and the protein concentration was determined with BCA kit according to the manufacturer's instructions. For digestion, the protein solution was reduced with 5 mM dithiothreitol for 30 min at 56°C and alkylated with 11 mM iodoacetamide for 15 min at room temperature in darkness. The protein sample was then diluted by adding 100 mM TEAB to urea concentration less than 2M. Finally, trypsin was added at 1:50 trypsin-to-protein mass ratio for the first digestion overnight and 1:100 trypsin-to-protein mass ratio for a second 4-h digestion. To enrich propionylation-modified peptides, tryptic peptides dissolved in NETN buffer (100 mM NaCl, 1 mM EDTA, 50 mM Tris-HCl, 0.5% NP-40, pH 8.0) were incubated with prewashed antibody beads (PTM202, PTM Bio) at 4°C overnight with gentle shaking. Then the beads were washed four times with NETN buffer and twice with H_2O. The bound peptides were eluted from the beads with 0.1% trifluoroacetic acid. Finally, the eluted fractions were combined and vacuum-dried. For HPLC-MS/MS analysis, the resulting peptides were desalted with C18 ZipTips (Millipore) according to the manufacturer's instructions.

The tryptic peptides were dissolved in 0.1% formic acid (solvent A), directly loaded onto a home-made reversed-phase analytical column (15 cm length, 75 μm i.d.). The gradient was comprised of an increase from 6% to 23% solvent B (0.1% formic acid in 98% acetonitrile) over 26 min, 23%–35% in 8 min, and climbing to 80% in 3 min then holding at 80% for the last 3 min, all at a constant flow rate of 400 nL/min on an EASY-nLC 1000 UPLC system. The peptides were subjected to NSI source followed by tandem mass spectrometry (MS/MS) in Q ExactiveTM Plus (Thermo) coupled online to the UPLC. The electrospray voltage applied was 2.0 kV. The m/z scan range was 350–1800 for full scan, and intact peptides were detected. The resulting MS/MS data were processed using Maxquant search engine (v.1.5.2.8). Tandem mass spectra were searched against the *Danio rerio* database concatenated with a reverse decoy database. Trypsin/P was specified as cleavage enzyme allowing up to four missing cleavages. The mass tolerance for precursor ions was set as 20 ppm in first search and 5 ppm in main search, and the mass tolerance for fragment ions was set as 0.02 Da. Carbamidomethyl on Cys was specified as fixed modification, and propionylation modification and oxidation on Met were specified as variable modifications. FDR was adjusted to <1%, and minimum score for modified peptides was set >40.

Cell viability analysis

ZF4 cell was first seeded on 96-well plates and incubated for 24 h to sub-confluence. Then ZF4 cell was exposed to fresh medium added with a mixture of 150 μM oleic acid and 50 μM palmitic acid (OPA) and a mixture of OPA and increasing concentrations of propionate (OPP). At the end of the exposure period, fresh medium with 10% AlarmaBlue cell viability reagent (Invitrogen, Grand Island, NY, USA) was added. After a 1-h incubation, fluorescence was measured with the SynergyH1 microplate reader (Biotek) at

excitation and emission wavelengths of 485 nm and 595 nm, respectively. The ratio of cell viability was calculated using the fluorescence readings of the OPA and OPP treatments.

Cell apoptosis analysis

Cell apoptosis detection was performed with Annexin V-fluorescein isothiocyanate (FITC) kits (Sigma). After exposure to OPA or OPP for 24 h, the cells were collected and incubated with Annexin V-FITC and propidium iodide in binding buffer for 10 min in darkness at room temperature. The analysis was conducted by the Guava easyCyte Flow Cytometer (Merck Millipore, Stafford, VA, USA).

Cellular ROS determination

Relative amount of cellular ROS was determined in ZF4 cells by using a fluorometric intracellular ROS kit (Sigma, USA). After exposure to OPA or OPP for 24 h, 100 μL/well of reaction mix containing ROS fluorogenic sensor was added into the 96-well black plate. After a 2-h incubation, the fluorescence was acquired with excitation and emission wavelengths of 490 nm and 520 nm, respectively. The relative fluorescence of ROS was calibrated by cell viability. ROS level was expressed as the fold change of the OPA group. The mean fluorescence intensity of ROS signal was detected by using a fluorescent probe DCFH-DA. After exposure to OPA or OPP for 24 h, ZF4 cell was incubated with DCFH-DA for 30 min and then harvested for fluorescence detection. The analysis was conducted by the Guava easyCyte Flow Cytometer (Merck Millipore, Stafford, VA, USA). The mean fluorescence intensity of ROS signal was expressed in MFI/5000 cells.

Determination of ROS in gut content and cell medium

Fresh gut contents were homogenized in cold PBS. The homogenates were then centrifuged at 11,000 g for 15 min at 4°C, and the supernatant was used for the measurement of ROS. The process of sample preparation is no more than 30 min. Cell medium was centrifuged at 11,000 g for 15 min at 4°C, and the supernatant was used for the measurement of ROS. Then both gut content and cell medium supernatants were incubated with fluorogenic sensor provided by a commercial kit (Sigma, USA) for 2 h to detect the relative level of ROS. This fluorogenic sensor could react with ROS and result in a fluorometric product, which could be detected by fluorescence microplate reader with excitation and emission wavelengths of 490 nm and 520 nm, respectively. The relative ROS level in gut content was expressed as the fold change of the HFD group. The relative ROS level in cell medium was expressed as the fold of OPA group.

Gene silencing with *si*RNA

Scrambled *si*RNA (negative control), *sod2*, and *sirt3 si*RNA (Table S5) were synthesized by GenePharma Co. Ltd. (Shanghai, China). Cells were first seeded on 6-well plates (Corning) and incubated for 24 h to subconfluence. Then the cells were transfected with the appropriate *si*RNAs using Lipofectamine RNAiMAX Transfection Reagent (Invitrogen). Efficiency of the *si*RNA was determined by *q*PCR.

In vitro propionylation assay

In vitro propionylation assay was carried out following established protocols (Liu et al., 2020) with minor modification. The reactions consist of propionylation buffer containing 20 mM HEPEs, 0.1 mg/mL BSA, 1 mM DTT, 3 μg purified Sod2, propionyl-CoA (0, 0.2, 0.4, 0.8, 1, 5 mM), 1 mM PMSF, and 1 × phosphatase inhibitor. Reaction mixture was incubated at 30°C for 2 h.

Plasmid construction and transfection

The Sod2 was cloned into *p*CDNA3.1 and generated *p*CDNA3.1-flag-Sod2. Point (Site) mutations of Sod2 (*p*CDHA3.1-flag-Sod2 132K/Q and *p*CDHA3.1-flag-Sod2 132K/R) were generated by QuikChange Site-Directed Mutagenesis kit (Stratagene). Both WT Sod2 and Sod2 mutant plasmids were transfected into ZF4 cells using Lipofectamine 3000 Transfection Reagent (Invitrogen). For protein purification, His tag was added to *p*CDNA3.1-flag-Sod2 to generate *p*CDNA3.1-his-flag-Sod2 and overexpressed in HEK293 cells.

Gut microbiota analysis

The *16s* V3–V4 region was amplified using the primers U341F (5′-CGGCAACGAGCGCAACCC-3′) and U806 (5′-CCATTGTAGCACGTGTGTAGCC-3′). The 16S ribosomal RNA gene sequencing was performed by Novogene Bioinformatics Technology Co. Ltd (Beijing, China) using the Illumina HiSeq platform. Then the raw

pair-end readings were subjected to a quality-control procedure using the UPARSE-operational taxonomic unit (OTU) algorithm (Edgar., 2013). The qualified reads were clustered to generate OTUs at the 97% similarity level using the USEARCH sequence analysis tool (Edgar., 2010). A representative sequence of each OTU was assigned to a taxonomic level in the Ribosomal Database Project (RDP) database using the RDP classifier (Maidak et al., 1997).

Germ-free zebrafish generation and treatment

Germ-free (GF) zebrafish were derived from normal zebrafish and reared following established protocols (Rawls et al., 2006). Zebrafish larvae hatched from their chorions at 3 days postfertilization (dpf). Each group had six bottles with 20 fish per bottle. At 5 dpf, the yolk was largely absorbed, and the GF-zebrafish was subjected with feeding of LFD, HFD, and HFSP0.5 or transfer of gut microbiota deprived from adult zebrafish fed LFD, HFD, and HFSP0.5. At 12 dpf, GF zebrafish fed LFD, HFD, and HFSP0.5 were collected for living ROS detection. At 8 dpf, zebrafish larvae transferred with LFD, HFD, and HFSP0.5-gut microbiota were collected for ROS detection, enzymes detection, and *q*PCR.

Detection of ROS in whole zebrafish larvae

The detection of ROS in whole zebrafish larvae was conducted following a Novel procedure (Lackmann et al., 2018). In brief, zebrafish larvae were washed twice with GF-zebrafish medium (GZM) and incubated with 5 μM DCFH-DA for 30 min. After the exposure to DCFH-DA, larvae were washed twice with GZM and placed individually on a drop of 3% methyl cellulose poured onto a microscope glass slide. The texture of methyl cellulose made sure that the larvae kept still. Images of zebrafish larva were obtained with Zeiss stereoscopic microscope (AXIO Zoom. V16). Image analysis and quantification were performed using ImageJ.

In vitro culture of gut microbiota and quantification

Fresh gut content samples pooled from five zebrafish were put on ice and diluted in 5 mL sterile, ice-cold PBS. Within 30 min of sample collection, bacteria were seeded into Gifu anaerobic medium (GAM): GAM supplemented with 2 mmol/L H_2O_2 (GAM + H_2O_2); GAM supplemented with 2 mmol/L H_2O_2 and 0.05% LA (GAM + H_2O_2+LA). After an incubation period of 48 h at 28°C, the number of total bacteria or a specific phylotype was quantified by *q*PCR according to Zhang et al. (Zhang et al., 2019). In brief, bacterial DNA were extracted from equal volume of bacterial culture (2 mL) by using a TIANamp Bacteria DNA kit (Tiangen, Beijing, China). Then the extracted DNA were subjected *q*PCR by using primers set for universal bacteria or specific bacterial groups targeting the 16S *r*DNA gene (Table S6). 16S rDNA of each bacterial strain was cloned into the pLB vector (Tiangen, Beijing, China) as a copy number standard. For each *q*PCR standard, the copy number concentration was calculated based on the length of the PCR product and the average mass of a DNA base pair. For the gut microbiota cultured *in vitro*, results were expressed as Log10 copy numbers of bacterial 16S *r*DNA per mL medium (Log_{10} copies · mL medium^{-1}).

Detection of ROS in gut microbiota medium

Gut microbiota from LFD, HFD, and HFSP0.5-fed zebrafish were cultured in GAM. At 24 h and 48 h, bacteria were collected by centrifuging at 12,000 g for 5 min, and supernatants were subjected to ROS detection with fluorogenic sensor provided by a commercial kit (Sigma, USA) for 2 h. The fluorometric product could be detected by fluorescence microplate reader with excitation and emission wavelengths of 490 nm and 520 nm, respectively. The relative ROS level in bacteria cultures was calibrated by bacteria population in each culture.

Western blotting

Zebrafish intestine or larval zebrafish were homogenized in ice-cold HBSS buffer mixed with 1 mM PMSF and phosphatase inhibitors. Equivalent amounts of total protein were loaded into a 12% SDS-PAGE for electrophoresis and then transferred into a PVDF membrane (Millipore, USA). After blocking nonspecific binding with 5% skimmed milk in TBST, the PVDF membrane was incubated with primary antibodies, i.e., antibodies against zebrafish Gapdh (Sigma, SAB2708126, 1:2000), Sod2 (Genetex, GTX124294, 1:1000), Sirt3 (Sigma, AV32388, 1:1000), Mtco1 (Abcam, ab14109, 1:2000), acetylated lysine (Cell Signaling Technology, 9441, 1:1000), and customized Sod2 K132pro (Jingjie PTM BIO, 1:500). The blots were developed using HRP-conjugated secondary antibodies (GE Health, 1:3000) and the ECL-plus system.

Total RNA extraction, reverse transcription, and *q*PCR

Total RNA was isolated using Trizol reagent and then reverse transcribed to cDNA. The *q*PCR was performed using SYBRGreen Supermix according to the manufacturer's instructions (Tiangen, Beijing, China). The results were stored, managed, and analyzed via LightCycler 480 software (Roche, Basel, Switzerland). The *q*PCR primers used are listed in Table S6.

QUANTIFICATION AND STATISTICAL ANALYSIS

All of the statistical analyses were conducted using GraphPad Prism 5 software (GraphPad Software Inc., San Diego, CA, USA). Results are expressed as the means ± standard errors of the means (SEMs). Comparisons between two groups were analyzed using the Student's t test, and comparisons between multiple groups were analyzed using one-way ANOVA followed by a Duncan's test. The statistical significance was set at $p < 0.05$. The number of replicates for each experiment are indicated in the figure legends.